NGC 6819: testing the asteroseismic mass scale, mass loss, and evidence for products of non-standard evolution

Handberg, R.; Brogaard, K.; Miglio, A.; Bossini, D.; Elsworth, Y.; Slumstrup, D.; Davies, Guy; Chaplin, W.~J.

DOI:
10.1093/mnras/stx1929

NGC 6819: testing the asteroseismic mass scale, mass loss, and evidence for products of non-standard evolution

R. Handberg[1,2⋆], K. Brogaard[2], A. Miglio[1,2], D. Bossini[1,2], Y. Elsworth[1,2]
D. Slumstrup[2], G. R. Davies[1,2], W. J. Chaplin[1,2]
[1] *School of Physics and Astronomy, University of Birmingham, Edgbaston, Birmingham B15 2TT, United Kingdom*
[2] *Stellar Astrophysics Centre (SAC), Department of Physics and Astronomy, Aarhus University, DK-8000 Aarhus C, Denmark*

Received <date> / Accepted <date>

ABSTRACT

We present an extensive peakbagging effort on *Kepler* data of ∼50 red giant stars in the open star cluster NGC 6819. By employing sophisticated pre-processing of the time series and Markov Chain Monte Carlo techniques we extracted individual frequencies, heights and linewidths for hundreds of oscillation modes.

We show that the 'average' asteroseismic parameter $\delta\nu_{02}$, derived from these, can be used to distinguish the stellar evolutionary state between the red giant branch (RGB) stars and red clump (RC) stars.

Masses and radii are estimated using asteroseismic scaling relations, both empirically corrected to obtain self-consistency as well as agreement with independent measures of distance, and using updated theoretical corrections. Remarkable agreement is found, allowing the evolutionary state of the giants to be determined exclusively from the empirical correction to the scaling relations. We find a mean mass of the RGB stars and RC stars in NGC 6819 to be $1.61 \pm 0.02\,\mathrm{M}_\odot$ and $1.64 \pm 0.02\,\mathrm{M}_\odot$, respectively. The difference $\Delta M = -0.03 \pm 0.01\,\mathrm{M}_\odot$ is almost insensitive to systematics, suggesting very little RGB mass loss, if any.

Stars that are outliers relative to the ensemble reveal overmassive members that likely evolved via mass-transfer in a blue straggler phase. We suggest that KIC 4937011, a low-mass Li-rich giant, is a cluster member in the RC phase that experienced very high mass-loss during its evolution. Such over- and undermassive stars need to be considered when studying field giants, since the true age of such stars cannot be known and there is currently no way to distinguish them from normal stars.

Key words: methods: data analysis – stars: oscillations

1 INTRODUCTION

Red giant stars in open clusters observed by the *Kepler* mission (Borucki et al. 2010; Borucki 2016) have already been the subject of several asteroseismic studies (see e.g. Basu et al. 2011; Stello et al. 2011; Corsaro et al. 2012; Miglio et al. 2012). Asteroseismology of ensembles of giants with similar parameters and a common age and metallicity has allowed new insights into the clusters and stellar evolution, examples being asteroseismic membership information (Stello et al. 2011), mass loss on the red giant branch (RGB) (Miglio et al. 2012) and stars with a non-standard evolutionary history (Corsaro et al. 2012; Brogaard et al. 2015, 2016). The asteroseismic studies of *Kepler* cluster giants to date are based on so called average asterseismic parameters and in the most detailed case on measurements from collapsed echelle diagrams (Corsaro et al. 2012) or by fitting an asymptotic expression (Vrard, Mosser & Samadi 2016). The next logical step, detailed peakbagging, meaning the extraction of individual oscillation modes and all their characteristics, has only been performed for a handful of stars in general and until now not for cluster members. The discipline has proven itself extensively for main-sequence and sub-giant stars (see e.g. Handberg & Campante 2011; Appourchaux et al. 2012b,a, 2014; Davies et al. 2016), but has not been applied to a large extent to evolved red giants (Corsaro, De Ridder & García 2015). This has mainly been due to complications introduced by the many mixed dipole modes. Here we present the first peakbagging effort on *Kepler* light curves of evolved red giant stars in the open star cluster NGC 6819.

In §2 and §3 we present the procedures used to prepare

⋆ E-mail: rasmush@phys.au.dk

the *Kepler* data for asteroseismic analysis and the methods used to extract global asteroseismic parameters from these. In §4 we use asteroseismic information to distinguish between evolutionary states. In §5 we go into detail on the peakbagging of individual oscillation modes, and in §6 we use these results to derive new robust global oscillation parameters, and perform the same analysis for the Sun in §7. In §8 and §9 we derive stellar properties and look into special cases of stars showing signs of non-standard evolution. Finally we summarize the results and draw conclusions in §10.

2 DATA PREPARATION

The targets of our study are mainly those of Stello et al. (2011), most of which were also studied by Corsaro et al. (2012). We excluded a few stars for different reasons, being colours that were very significantly off compared to the cluster sequence in the colour-magnitude diagram (CMD), a high peak not related to solar-like oscillations in the power spectrum, or a very low $\nu_{\rm max}$ where measurements are extremely challenging ($\lesssim 4\,\mu$Hz). The stars for which we made measurements are listed in Table A1 and shown in the CMD of Fig. 3 based on photometry from Milliman et al. (2014); Hole et al. (2009) and Cutri et al. (2003a) with labels as determined throughout this paper.

Kepler observations are divided into 'quarters' of approximately 3 months duration due to the roll of the spacecraft required to keep the solar panels pointing towards the Sun. In this work we have used *Kepler* data taken in long cadence (29.4 min) from observing quarters Q0–Q16. NGC 6819 falls on *Kepler* CCD module 3, which failed after the first year of operation (Q4). This means that the time series of NGC 6819 is unfortunately missing data for 3 months every year, but have otherwise been near continuously observed.

The raw *Kepler* data was preprocessed using the procedures described in Handberg & Lund (2014). Normally this procedure involves using the *Kepler* target pixel data to automatically redefine the pixel masks used for extracting the stellar flux using simple aperture photometry. This is to allow more flux from the target through the aperture and has been shown for field stars to improve asteroseismic analyses compared to the *Kepler* standard masks. However, since we are here dealing with a relatively crowded field, this procedure was not ideal for all targets and all timeseries were therefore visually inspected to decide if the new or original masks performed better for each target with respect to contamination and overall scatter.

From initial analyses of the data and previously published asteroseismic parameter values (Stello et al. 2011), we had initial indications of the frequency ranges in which the stars oscillate, and care was taken to scale the filter parameters in such a way that the oscillation signals would not be perturbed in any way (see Handberg & Lund 2014).

3 GLOBAL ASTEROSEISMIC PARAMETERS

The acoustic oscillation frequencies of solar-like stars are approximatively described by (Tassoul 1980):

$$\nu_{n\ell} \simeq \Delta\nu(n + \ell/2 + \varepsilon) - \delta\nu_{0\ell}\,, \tag{1}$$

where n and ℓ denote the radial order and spherical degree of the oscillation mode respectively, $\Delta\nu$ is the large frequency separation, ε is an offset introduced by surface effects and $\delta\nu_{0\ell}$ is the small frequency separation.

The power spectrum of a solar-like oscillator is dominated by an overall background arising primarily from the turbulent convective motions in the outer layers of the star. This convective motion drives the acoustic oscillations in the star, often referred to as the p-modes of oscillation. The measured power spectrum of a solar-like oscillator will therefore consist of individual peaks from each mode of oscillation sitting on top of the granulation background signal. These modes will exhibit a regular pattern with the distance between consecutive overtones of approximately $\Delta\nu$. The first step in the analysis of a solar-like oscillator is to fit and describe the background signal. However, since there does not exist any physically founded description for the true shape and size of the granulation signal, it is common practice to turn to an empirical description. Historically, following the principles in Harvey (1985), the background is described as the sum of several Lorentzian (or super- or pseudo-Lorentzian) functions. This choice stems from the empirical description of the brightness of the granules that falls of exponentially.

In this work we have opted for not selecting *a priori* any particular model for the background, but instead the backgrounds are fitted, using maximum a posteriori probability estimation, using four different and commonly used descriptions of the background signal (Harvey 1985; Karoff 2008; Kallinger et al. 2012; Karoff et al. 2013; Kallinger et al. 2014):

$$N(\nu) = \eta(\nu) \cdot \sum_{k=1}^{2} \frac{\xi\sigma_k^2\tau_k}{1 + (2\pi\nu\tau_k)^2} + K \tag{2}$$

$$N(\nu) = \eta(\nu) \cdot \sum_{k=1}^{2} \frac{\xi\sigma_k^2\tau_k}{1 + (2\pi\nu\tau_k)^4} + K \tag{3}$$

$$N(\nu) = \eta(\nu) \cdot \sum_{k=1}^{2} \frac{\xi\sigma_k^2\tau_k}{1 + (2\pi\nu\tau_k)^2 + (2\pi\nu\tau_k)^4} + K \tag{4}$$

$$N(\nu) = \eta(\nu) \cdot \sum_{k=1}^{2} \frac{\xi\sigma_k^2\tau_k}{(1 + (2\pi\nu\tau_k)^2)^2} + K \tag{5}$$

where σ_k and τ_k is the amplitudes and time-scales of each component, ξ is a normalisation constant, and K is the white noise level. The frequency dependent factor $\eta(\nu) \equiv \mathrm{sinc}^2(\Delta T_{\rm int} \cdot \nu)$ is the attenuation arising from gathering the data over a time-span, $\Delta T_{\rm int}$ (the exposure time), which in the case of *Kepler* long cadence data is 1765.5 s. sinc is the normalized sinc-function: $\mathrm{sinc}(x) = \sin(\pi x)/(\pi x)$. In addition to this comes a Gaussian envelope accounting for the oscillation power. The location of the highest point in this envelope is defined as $\nu_{\rm max}$, and the resulting combined model

power spectrum is defined as follows:

$$\mathscr{P}(\nu) = N(\nu) + \eta(\nu)\, a_{\rm env} \exp\left[\frac{-(\nu-\nu_{\rm max})^2}{2\sigma_{\rm env}^2}\right], \quad (6)$$

where $a_{\rm env}$ and $\sigma_{\rm env}$ is the height and width of the envelope respectively. This model is fitted to the full power spectrum. The large separation, $\Delta\nu_{\rm global}$, is then estimated by the use of the power spectrum of the power spectrum (PSPS; see Handberg 2013) in the frequency range $\nu_{\rm max} \pm 2\sigma_{\rm env}$. The model is fitted with constraints based on initial guesses on $\nu_{\rm max}$ and $\Delta\nu$ (from visual inspection) and in each case, the background fit and large separation calculation are iterated three times to yield a consistent result. Finally the background with the lowest Bayesian Information Criterion (BIC; Schwarz 1978) is chosen as the adopted background:

$$\mathrm{BIC} = -2\ln\mathcal{L} + k\cdot\ln N\,, \quad (7)$$

where $\mathcal{L}$ is the calculated maximum likelihood from the best fit, k is the number of degrees of freedom and N is the number of points in the power spectrum being fitted. It should be noted that the BIC is an approximation to the true Bayesian evidence, and only valid when the data distribution is in an exponential family, but this is also the case for power spectra. Once the optimal shape of the background has been chosen, the fitted parameters are passed as first guesses to a Markov chain Monte Carlo method (Handberg & Campante 2011) which yields the final values of the parameters and corresponding error estimates.

The reason for not choosing a fixed background model *a priori* is that, prior to comparing with the data, we do not have any preference for any specific empirical model. Fixing the background to a single model for all stars comes with the prior assumption that the exact shape of the granulation background is well known and static for all stars – a statement which appears premature, although our understanding of granulation has significantly progressed in recent years (see e.g. Trampedach et al. 2013, 2014).

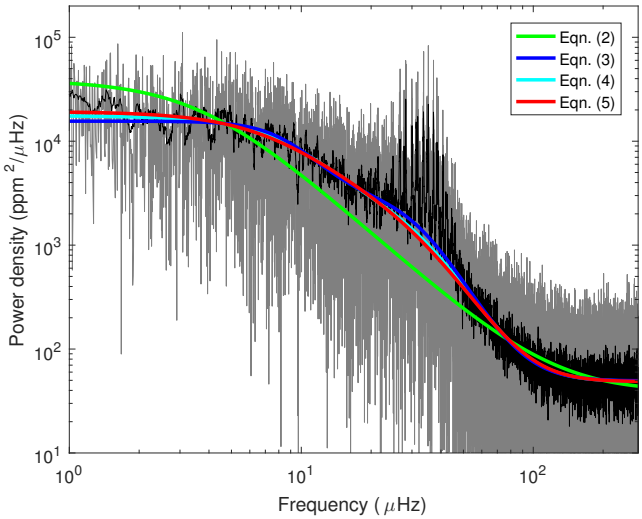

Figure 1. Power density spectrum and all the fitted background models for KIC 4937576 ($\nu_{\rm max}$ = 33 µHz). In gray the original power density spectrum and in black the same spectrum smoothed with a 0.14 µHz wide boxcar. Eq. 4 was the preferred background model for this star.

Fig. 1 shows the power density spectrum of KIC 4937576 with all the different background models considered overplotted. The preferred background model for this particular target is Eq. 4. What can also be seen from this is that Eqns. 3–5 are very similar, but Eq. 2 reproduces the background-level very poorly in this case.

Fig. 2a shows the BIC for each background model for all stars sorted by $\nu_{\rm max}$. The model with the lowest value of BIC was used in the further analysis. As seen from Fig. 2a, there seems to be a slight correlation between which background model is preferred as a function of stellar evolution ($\nu_{\rm max}$). Disregarding Eq. 2, which overall does a poor job of describing the power spectra, Eq. 3 seems to perform better at low $\nu_{\rm max}$ until roughly the location of the red clump (RC) ($\nu_{\rm max}$=30–50 µHz) and at higher $\nu_{\rm max}$ Eq. 5 is in general preferred. Eq. 4 in general lies between these two in terms of BIC. Of course, care has to be taken in drawing too firm conclusions from this, since the BIC is only a measure of how well the models describe a given dataset. It does not necessarily say anything about the validity of the background models in general.

Since the most important parameter of these fits is $\nu_{\rm max}$, a very important question then arises: Does the determined value of $\nu_{\rm max}$ depend on which background model we use? We have therefore fitted the power spectra using the different background-prescriptions, but without selecting only the best one. In Fig. 2b the relative difference between the returned $\nu_{\rm max}$ are shown. It is clear that there are significant deviations between Eq. 2 and the other models at low $\nu_{\rm max}$. But since this model is never selected for low $\nu_{\rm max}$ this has no impact on the returned $\nu_{\rm max}$. In general the differences between the returned values of $\nu_{\rm max}$ are almost all consistent with zero within the errorbars. This means that the values of $\nu_{\rm max}$ are largely independent of which background model is used, with the exception of Eq. 2.

We also tested the background model proposed by Kallinger et al. (2014). This model is identical to Eq. 3, but with the addition of an "instrumental" component, increasing the number of free parameters by two, which is penalised in the BIC. In the best cases it performed as well as Eq. 3, but often significantly worse, particularly at low $\nu_{\rm max}$. We also observed larger deviations in $\nu_{\rm max}$ when using this model when compared to the other models. For a subset of we also observed problems of getting the fit to converge. We also ascribe this to the additional free parameters.

4 PERIOD SPACINGS AND CLASSIFICATIONS

The evolutionary state classification is mainly based on the appearance of the mixed-mode structure of the dipole modes in the power spectrum. The procedure is described in detail in Elsworth et al. (2016), but the outline is as follows.

We use the previously determined value of $\Delta\nu$ to divide the spectrum into zones in which either odd or even ℓ modes are located. Within each zone we then use statistical tests on the unsmoothed spectrum to pick out significant spikes. The significance threshold is set so as to exclude almost all the background noise but to pick up small features in the spectrum.

This is a frequentist approach that makes no assump-

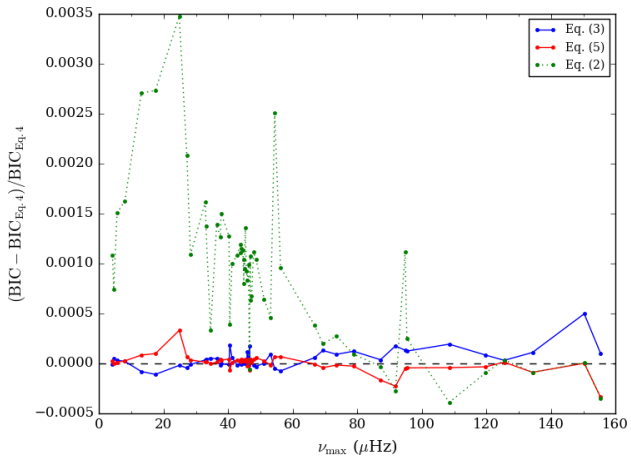

(a)

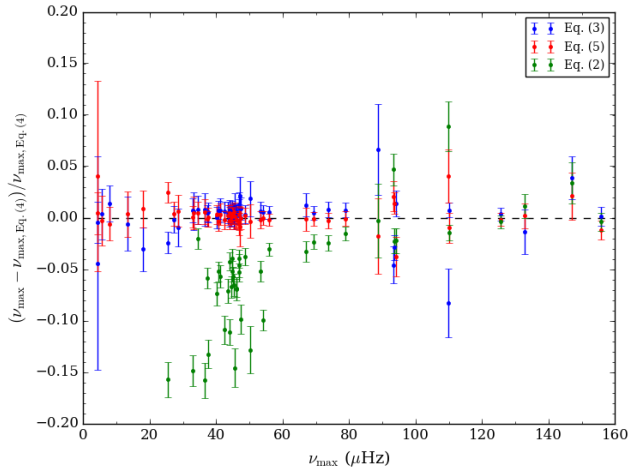

(b)

Figure 2. (a): Bayesian Information Criterion (BIC) for different background models. For each star, the background model with the lowest BIC was used in the following analysis. (b): Comparison of ν_{max} for different background models.

tions about what will be present in the data. The result of the test is a set of frequencies at which spikes have been found. The criterion employed is that a feature is considered significant if there is a less than 20% probability of a false detection over a frequency range of 3.5μHz. This range represents a typical $\Delta\nu$ for a RC star.

In each zone, we find the separation in frequency of each feature from all other features. Thus, if there were x features identified from the statistical tests there would be $x(x-1)$ frequency differences. A histogram is formed from these which gives the number of occurrences of different frequency differences. The features to be found in these histograms carry information about the features within the spectrum and are different in the two zones of odd and even ℓ. The classification uses just the odd ℓ zone. The histogram of the odd-ℓ zone will show the large frequency separation but will additionally show features that are a consequence of the presence of mixed modes.

Core-helium burning stars tend to show several mixed modes of similar heights over many orders with observed period spacings that typically lie between about 100 s and 250 s. For RGB stars, the period spacing is much smaller at around 60 s and the mixed modes have a sufficiently large inertia that they are not always visible (see e.g. Bedding et al. 2011; Mosser et al. 2012b). These properties influence the features in the frequency difference histogram. Furthermore, by definition, the asymptotic period spacing is uniform in period and not in frequency. This means that the frequency difference between two mixed modes at the low-frequency end of the spectrum is significantly smaller than the difference at the high-frequency end. This variation influences the width of the feature in the frequency-separations which, expressed as a function of $\Delta\nu$, can be used to differentiate the two classes of red giants. More details on the method are given in Elsworth et al. (2016).

Stars which have depressed dipole modes cannot be classified in this way. Therefore, a few stars were instead classified by their CMD positions and according to their small spacing $\delta\nu_{02}$, see 6.

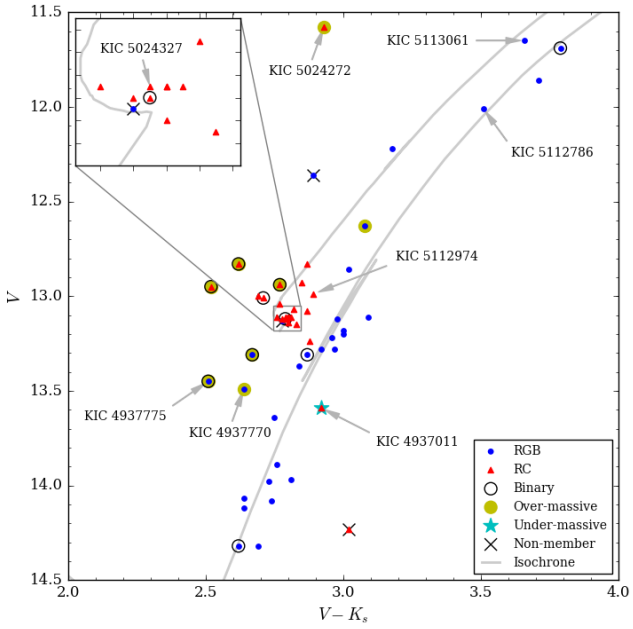

Figure 3. Colour-magnitude diagram of the observed giants in NGC 6819. The isochrone is from PARSEC (Bressan et al. 2012).

5 PEAKBAGGING

From a simple look at the power spectra of the stars in NGC 6819 and in particular on the structure of the dipole modes of these, it becomes apparent that these can be empirically divided into three groups: Low RGB, RC, and "clean dipole" stars. In Fig. 4 the power spectra of representative stars for each of the three groups are shown. The low RGB stars, which are stars with $\nu_{\mathrm{max}} \gtrsim 60\mu$Hz, are characterized by having rich spectra with many mixed dipole modes. In some of them rotational splitting is visible, but reasonably distinguishable from the mixed mode structure as the rotational splittings are still smaller than the observed period spacings. For the RC stars, which lie in the

region $\nu_{\rm max}$ ≈35–45μHz, the power spectra are also very rich in structure. However, for these stars the asymptotic dipole structure is not always as clear. This may simply be because rotational splitting, which is now on the same scale as the period spacings, is complicating the spectra. The last group, the "clean dipole" stars, are evolved RGB stars with $\nu_{\rm max} \lesssim 60$μHz and power spectra which are very reminiscent of main-sequence stars. Each order apparently only contains a single dipole mode with a shape similar to the radial modes, sitting roughly where you would expect it from the asymptotic description (Eq. 1). From stellar models we know that these dipole modes are in fact composed of several mixed dipole modes sitting very close together in frequency around the *nominal p-mode*, ν_p, meaning the frequency where the pure p-mode would sit if there was no mixing with g-modes. Each individual mode is not resolved in the power spectrum, but the combined power excess from them yields what appears as a single clean Lorentzian mode (see e.g. Dupret et al. 2009; Montalbán et al. 2010a).

For the different empirical groups of stars, we opted for slightly different strategies in which modes were included in the peakbagging. In all cases we included a single oscillation mode for each $\ell=0$ and $\ell=2$ modes. We know that in principle the $\ell=2$ may also contain mixed modes, but these are in general confined close together and hence unresolved. Both the mixed modes signatures and any rotational splitting will manifest in nearly symmetrical features in frequency and will not cause significant errors in the determined frequencies. It is however important to keep this in mind when comparing the parameters to stellar models and we add a note of caution that individual $\ell=2$ modes can be biased because of this.

Following the same line of thought, in the cases of the "clean dipole" stars, we have elected to fit the dipole modes with a single Lorentzian peak with frequency, linewidth and height as free parameters, but not including rotational splitting.

For the low RGB and RC stars, the regions between the $\ell = 0, 2$ mode pairs containing power from the dipole modes was taken out. This was done by simply not including these regions in the sum over all bins in the calculation of the log-likelihood between the model spectrum and the observed power spectrum. It is clear that we could include the individual mixed dipole if a clear mode identification could be obtained. In general this is very difficult in the red clump stars, but can be done for some of the low RGB stars. For cases where it was possible, for low RGB stars, we chose to include the individual dipole modes in the peakbagging, using the asymptotic relation from Mosser et al. (2012b) for the frequencies of mixed dipole modes, $\nu_{\rm mix}$, to set initial guesses. The relation which needs to be iteratively solved for $\nu_{\rm mix}$ is the following:

$$\nu_{\rm mix} \simeq \nu_p + \frac{\Delta\nu}{\pi} \arctan\left[q \tan\left(\frac{1}{\Delta\Pi_1 \nu_{\rm mix}}\right) - \varepsilon_g\right], \qquad (8)$$

where ν_p is the nominal p-mode frequency, q is the coupling, $\Delta\Pi_1$ is the asymptotic dipole period-spacing and ε_g is a phase shift. In addition to this, it is essential to include rotational splitting in order to describe the oscillation spectrum. We have included this following Goupil et al. (2013), where the rotational splitting of a mixed mode at $\nu_{\rm mix}$ is given by:

$$\delta\nu_s \approx \left(\frac{1-2\mathcal{R}}{1+4\frac{\Delta\Pi_1\nu_{\rm mix}^2}{\Delta\nu}\cos^2\left(\frac{\pi}{\Delta\Pi_1\nu_{\rm mix}}\right)} + 2\mathcal{R}\right)\delta\nu_{s,\rm max}\,, \qquad (9)$$

where $\mathcal{R}$ is defined as the ratio between the average rotation rate of the envelope and the core, $\mathcal{R} \equiv \langle\Omega\rangle_{\rm env}/\langle\Omega\rangle_{\rm core}$, and $\delta\nu_{s,\rm max}$ is the maximal rotational splitting of the most g-like modes. In order to find the values of the free parameters in Eq. 8 and Eq. 9 which best reproduce the observed spectrum, parameters were varied manually until good agreement was found between the peaks of the observed spectrum and the calculated frequencies. Once initial guesses were set using the above prescription, frequencies, linewidths and rotational splittings were fitted individually for all modes. See also Corsaro, De Ridder & García (2015) who performed peakbagging of this type of stars.

We fit the individual oscillation modes using the Markov chain Monte Carlo (MCMC) techniques described in Handberg & Campante (2011). The principle is to fit the observed power density spectrum with a model power spectrum that is defined as a simple sum of Lorentzian profiles and the background contribution:

$$\mathscr{P}(\nu) = \eta(\nu)\cdot\sum_{n,\ell}\sum_{m=-\ell}^{\ell}\frac{\mathcal{E}_{\ell m}(i)H_{n\ell}}{1+\frac{4}{\Gamma_{n\ell}^2}(\nu-\nu_{n\ell}-m\delta\nu_{s,n\ell})^2} + N(\nu)\,, \qquad (10)$$

where mode frequencies, heights, linewidths and rotational splittings ($\nu_{n\ell}$, $H_{n\ell}$, $\Gamma_{n\ell}$, $\delta\nu_s$) are all treated as independent free parameters. In the cases where rotation was not included in the fit, $\delta\nu_s=0$ and $\mathcal{E}_{\ell m}(i)=1$ were simply fixed.

Priors on mode frequencies and linewidths are set as uniform distributions (boundaries of which are defined on per-case basis). The prior on heights are set as modified Jeffreys priors (see e.g. Handberg & Campante 2011). The parameters for the background are also treated as free parameters, but with strong priors set as the posterior probability distributions of the background fit already made to the full frequency range.

After the fitting is done, all posterior probability distributions are inspected manually to reject any modes that could not be reliably fitted. For each posterior, the median value is chosen as the central value and the 1σ errorbars are calculated from the 68% credible region. This means that there is 68% confidence that the parameter will have its true value in this interval.

We did not correct the final oscillation frequencies for the line-of-sight Doppler velocity shifts as described in Davies et al. (2014). Although the radial velocity measurements are available for the individual stars, we are dealing with low-frequency oscillations and the cluster system velocity of only 2.45±1.02 km/s (Milliman et al. 2014) is low, rendering the corrections insignificant.

6 EXTRACTED AVERAGE SEISMIC PARAMETERS

Our goal is now to use the individual frequencies we have extracted from the detailed peakbagging to reconstruct the average seismic parameters of Eq. 1. This has the advantage

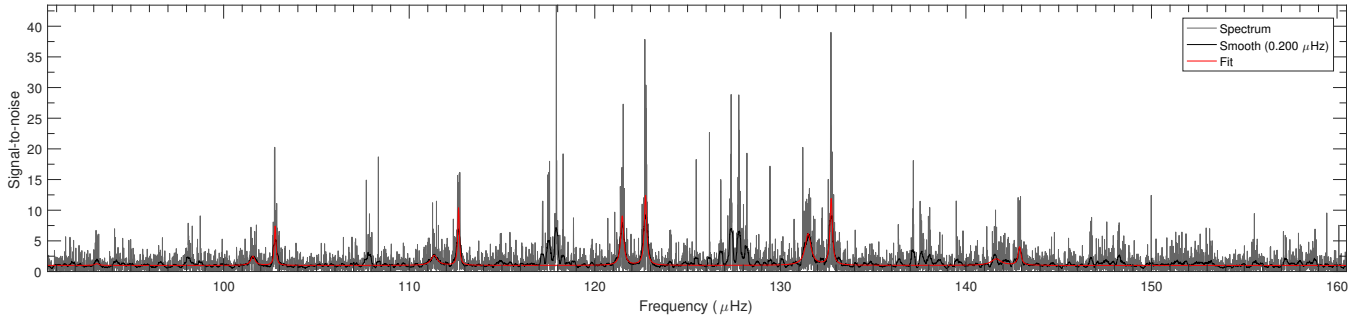

(a) KIC 5112072. Low Red Giant Branch star.

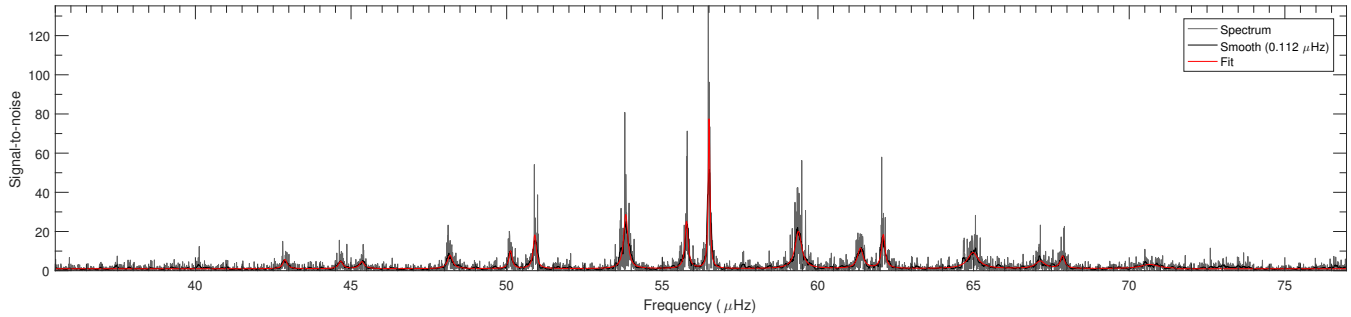

(b) KIC 5024043. "Clean dipole" star.

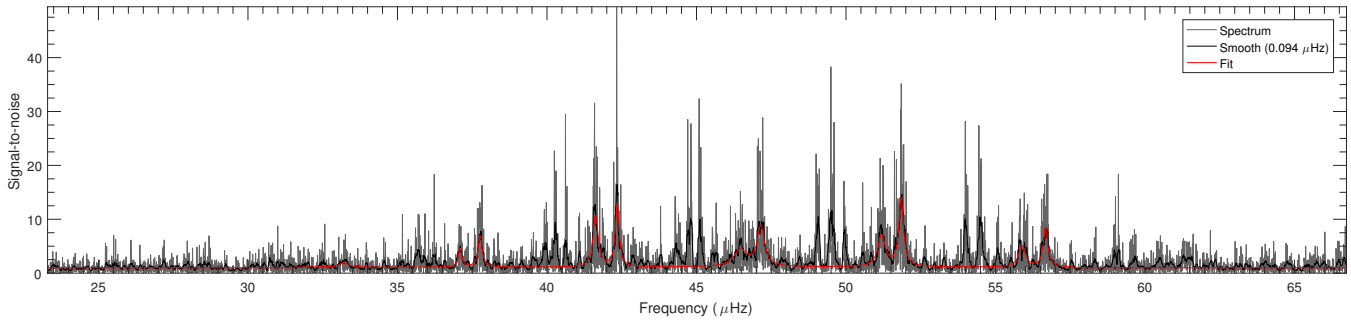

(c) KIC 5024327. Red Clump star.

Figure 4. Power spectra of representative stars of the three empirical types of stars in NGC 6819. Power spectra have here been divided by the fitted background model. The red line indicates the fitted limit spectrum (Eq. 6), using the medians of the posterior probability distribution.

that the same procedures can easily be applied to frequencies originating from stellar models, allowing for direct comparison. This is something that is, for example, not easily achievable with $\Delta\nu_{\rm global}$ derived from the autocorrelation of the measured power spectrum. From the extracted $\ell = 0, 2$ frequencies we can construct the average parameters $\Delta\nu_{\rm fit}$, ε and $\delta\nu_{02}$. The first two are found by a weighted linear fit to the extracted radial mode frequencies, where the weights are given as σ_i^{-2}, where σ_i is the uncertainty of the individual frequencies. The slope of the fitted curve directly gives $\Delta\nu_{\rm fit}$, while the intersection with the zero-axis yields ε. $\langle\delta\nu_{02}\rangle$ is found as the weighted mean of the frequency differences between adjacent $\ell = 2$ and $\ell = 0$ modes.

In Fig. 5 the values of $\Delta\nu_{\rm fit}$, determined from the measured individual frequencies, are compared to the values of $\Delta\nu_{\rm global}$, which as previously mentioned is measured using the PSPS. In general there is good agreement between the two estimates, which is reassuring for stars where individual frequencies can not be obtained. We do see some scatter at the 1% level, but well within the errorbars of the measurements.

As expected we find a strong correlation between the observed $\Delta\nu$ and $\nu_{\rm max}$ (see e.g. Stello et al. 2009; Huber et al. 2011). The scaling between the parameters obtained in this work, assuming the usual power-law dependence, is the following:

$$\Delta\nu_{\rm fit} = (0.248 \pm 0.009) \cdot \nu_{\rm max}^{(0.766\pm0.008)} . \qquad (11)$$

Comparing to others, it is important to note that this scaling is for a particular mass (the RGB mass of NGC 6819, which we derive later) and metallicity.

As previously mentioned, the second global asteroseismic parameter that we can estimate from the individual frequencies of the radial modes is the ε parameter, often refereed to as the "surface-term". Following Mosser et al. (2011) we determine the best fitting power function of the form $\varepsilon = a + b\log_{10}(\Delta\nu)$, which yields the following scaling

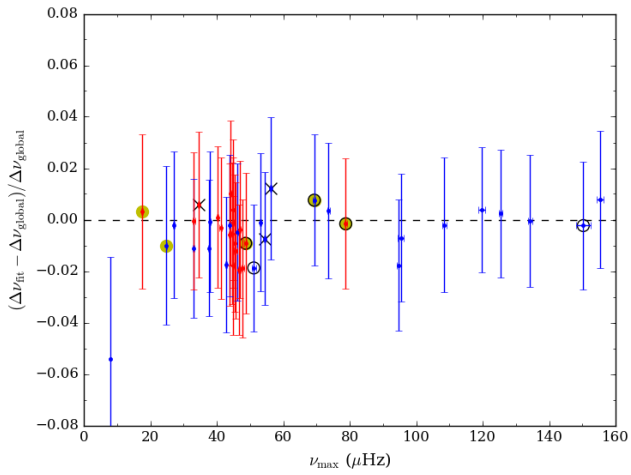

Figure 5. Comparison between $\Delta\nu_{\rm fit}$ and $\Delta\nu_{\rm global}$ in the cases where they could both be obtained. Colours and points are the same as in Fig. 3. This clearly shows that there is no significant difference between the two estimates, however some scatter on the ∼1% level is seen.

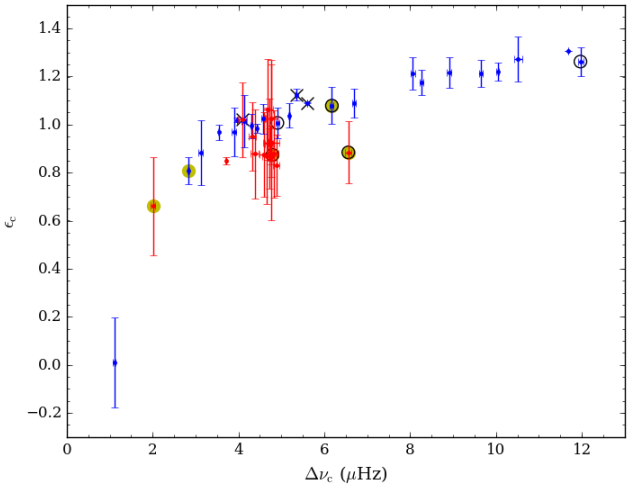

Figure 6. Seismic ε_c vs $\Delta\nu_c$ parameters determined from the three central, individually fitted, radial modes. Colours and points are the same as in Fig. 3. The reason for the, in general, larger errorbars on the RC stars is fact that RC stars have a more 'messy' power spectrum, as seen in Fig. 4, which translates into larger errorbars on the radial mode frequencies.

relation for ε:

$$\varepsilon = (0.634\pm0.040) + (0.612\pm0.048)\cdot\log_{10}(\Delta\nu_{\rm fit})\,. \quad (12)$$

The parameters of this fit are within the 1-σ errors of a similar scaling relation reported by Corsaro et al. (2012).

Kallinger et al. (2012) proposed and alternative definition where, unlike in the above mentioned prescription, only the three central radial modes closest to $\nu_{\rm max}$ are used to measure $\Delta\nu_c$ and ε_c (here indicated by the subscript). Kallinger et al. (2012) used this definition to determine the evolutionary phase of field stars. Both definitions of $\Delta\nu$ and $\Delta\nu_c$, and of ε and ε_c gives very similar results but, not surprisingly, the errorbars on ε are remarkably smaller, at the cost of not tracing the evolutionary differences. However, as we show in Fig. 6, ε_c is in our case also not able to separate the RGB stars from the RC stars particularly well. We do see the trend reported by Kallinger et al. (2012) that RC stars tend to have a smaller ε_c at $\Delta\nu$ ∼4–4.5μHz, but the distinction does not seem to be significant on an individual star basis due to a significant overlap in ε_c for the RC and RGB stars.

6.1 Small frequency separation

However, if we turn our attention to the parameter $\langle\delta\nu_{02}\rangle/\Delta\nu_{\rm fit}$ (see e.g. Montalbán et al. 2010b,a, 2012), the distinction between RGB and RC stars turns out to be more prominent. In Fig. 7b this quantity is shown as a function of the large frequency separation determined from stellar models and in Fig. 7a the same is shown for the measured values. It would appear the we have identified an alternate way to distinguish the RGB from the RC phase, since our measurements clearly separate the two evolutionary phases. As seen, this is also in very good agreement with our theoretical predictions for the red giant mass of NGC 6819 (see §8). However, while our model predictions for a lower mass of 1.1 $M_\odot$ suggest a similar difference in $\langle\delta\nu_{02}\rangle/\Delta\nu_{\rm fit}$ between the two evolutionary phases, the measurements by Corsaro et al. (2012) of giants in the old open cluster NGC 6791 showed an overlap where the $\langle\delta\nu_{02}\rangle/\Delta\nu_{\rm fit}$ of RC stars scattered on both sides of the RGB stars (see panel b of their Fig. 4). Since NGC 6791 is very metal-rich one could suspect this to be the cause of the disagreement. Luckily, our analysis of individual targets in §9.3 identified a non-member RC star of solar metallicity with a mass of 1.1 $M_\odot$ that allows us to test that hypothesis. We show that one measurement in Fig. 7b where it demonstrates the same issue; the value of $\langle\delta\nu_{02}\rangle/\Delta\nu_{\rm fit}$ does not follow the model prediction for a 1.1 $M_\odot$ RC star of solar metallicity. Although outside the scope of the present paper this clearly should be investigated further.

In Fig. 7c the solid line corresponds to a linear fit to the RGB stars given by the following expression:

$$\langle\delta\nu_{02}\rangle = (0.0504\pm0.0074) + (0.1179\pm0.0014)\cdot\Delta\nu_{\rm fit}\,, \quad (13)$$

plotted together with previously published scaling relations by Huber et al. (2010), Mosser et al. (2011) and Corsaro et al. (2012). The difference in $\langle\delta\nu_{02}\rangle$ between RGB and RC stars is similar to previous studies (see Fig. 7), but there are systematic offsets in the absolute numbers, which is most likely due to the different methods used to measure $\langle\delta\nu_{02}\rangle$.

We have also looked at the extracted average linewidth of the radial modes, and come to the conclusion that this shows no clear systematic variations as a function of evolutionary state. All stars have $\langle\Gamma_{n0}\rangle$ in the range 0.08–0.2 μHz. There could maybe be a very slight variation of the linewidth as a function of effective temperature as reported by Corsaro et al. (2012), but the correlation is not statistically significant from our given sample. See Fig. 8. The effective temperatures are derived in §8.

We add a note of caution that the measured linewidths of course will depend on the chosen noise background formulation (see e.g. Appourchaux et al. 2012a, 2014; Corsaro & De Ridder 2014).

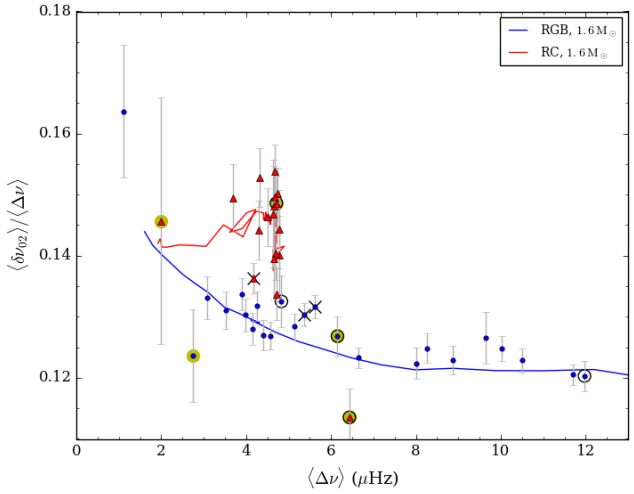

(a)

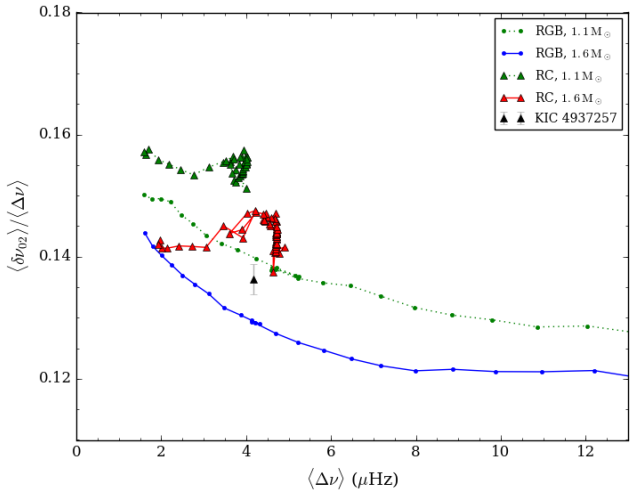

(b)

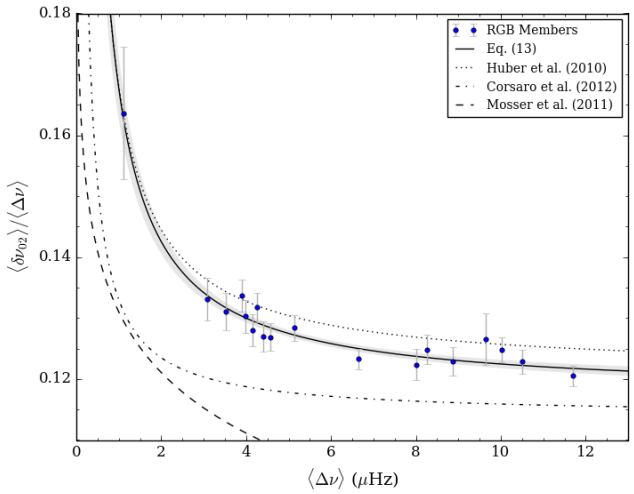

(c)

Figure 7. Small frequency separation as a function of large frequency separation. (a): Measured values for all stars overlaid with predictions from stellar models of 1.6 $M_\odot$. (b): Predictions from stellar models for two different masses. (c): Comparison between empirical scaling relations and RGB single cluster members. The shaded gray region denotes the 1-σ confidence interval around the fitted curve.

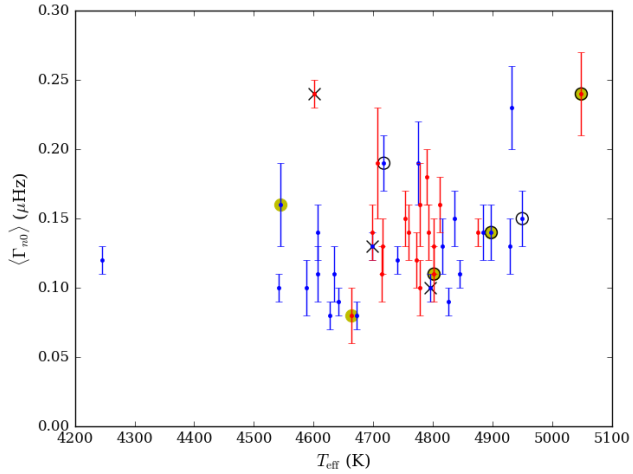

Figure 8. Average linewidth of radial modes as a function of effective temperature of the stars. Symbols have the same meaning as in previous figures. We do not see a significant correlation like reported by Corsaro et al. (2012). The effective temperatures are derived in §8.

7 SOLAR REFERENCE VALUES

In order to utilize scaling relations for the stellar parameters (see next section), we need values for $\nu_{\rm max}$ and $\Delta\nu$ of the Sun using similar methods to the ones used to obtain the values from the stars. To do this for $\nu_{\rm max}$ we fitted a 12 year power spectrum from the green channel of the VIRGO instrument aboard the SoHO spacecraft with the prescription given in §3. This yields a solar value for $\nu_{\rm max,\odot} = 3090\,\mu$Hz (Eq. 4). This value is in exact agreement with $\nu_{\rm max,\odot} = 3090\pm30\,\mu$Hz determined by Huber et al. (2011) who averaged 111 30-day subsets of the same data spanning from 1996 to 2005. It is also in close agreement with $\nu_{\rm max,\odot} = 3078 \pm 13\,\mu$Hz measured by Lund et al. (2017) using a weighted average of the green and red VIRGO channel to better match the *Kepler* bandpass for a 1150-day timestring with low activity level on the Sun (M. Lund, private communication). The most different measurement we have be able to find in the literature is the measurement of Gaulme et al. (2016) who find $\nu_{\rm max,\odot} = 3160 \pm 10\,\mu$Hz from a 49 day long VIRGO green channel time series. This suggests that a stable reference value is found as long as one uses a long time series.

We obtained our reference value for $\Delta\nu_\odot = 134.9 \pm 0.06\,\mu$Hz by fitting the the solar frequencies from BiSON (Broomhall et al. 2009), but using only $\ell = 0$ modes in the 6 central orders lying closest to the estimated $\nu_{\rm max}$ to mimic the procedure we apply to the the giants later. This value is in close agreement with $\Delta\nu_\odot = 135.1 \pm 0.1\,\mu$Hz (Huber et al. 2011), $\Delta\nu_\odot = 134.91 \pm 0.02\,\mu$Hz (Lund et al. 2017), and even $\Delta\nu_\odot = 134.82 \pm 0.08\,\mu$Hz from the short 49 day time series mentioned above (Gaulme et al. 2016).

Potential errors in our solar reference values for $\nu_{\rm max}$ and $\Delta\nu$ cause potential errors in mass and radius estimates from the asteroseismic scaling relations. If we take the largest differences between our values and those in the literature as estimates of the largest potential systematic error, these are of 6.9% and 2.3% from $\nu_{\rm max}$, and 0.3% and 0.2% from $\Delta\nu$, for mass and radius respectively.

8 TEMPERATURES, RADII, MASSES AND RGB MASS-LOSS

The fundamental stellar properties mass and radius can be estimated using the so-called asteroseismic scaling relations (Brown et al. 1991; Kjeldsen & Bedding 1995):

$$\frac{R}{\mathrm{R}_\odot} \simeq \left(\frac{\Delta\nu}{\Delta\nu_\odot}\right)^{-2}\left(\frac{\nu_{\rm max}}{\nu_{\rm max,\odot}}\right)\left(\frac{T_{\rm eff}}{T_{\rm eff,\odot}}\right)^{1/2} \quad (14)$$

$$\frac{M}{\mathrm{M}_\odot} \simeq \left(\frac{\Delta\nu}{\Delta\nu_\odot}\right)^{-4}\left(\frac{\nu_{\rm max}}{\nu_{\rm max,\odot}}\right)^{3}\left(\frac{T_{\rm eff}}{T_{\rm eff,\odot}}\right)^{3/2} \quad (15)$$

In the case of star clusters where we can obtain an independent distance estimate, and hence the luminosity of the stars L, the mass-scaling can also be written in three other ways (Miglio et al. 2012):

$$\frac{M}{\mathrm{M}_\odot} \simeq \left(\frac{\Delta\nu}{\Delta\nu_\odot}\right)^{2}\left(\frac{L}{\mathrm{L}_\odot}\right)^{3/2}\left(\frac{T_{\rm eff}}{T_{\rm eff,\odot}}\right)^{-6}, \quad (16)$$

$$\frac{M}{\mathrm{M}_\odot} \simeq \left(\frac{\nu_{\rm max}}{\nu_{\rm max,\odot}}\right)\left(\frac{L}{\mathrm{L}_\odot}\right)\left(\frac{T_{\rm eff}}{T_{\rm eff,\odot}}\right)^{-7/2}, \quad (17)$$

$$\frac{M}{\mathrm{M}_\odot} \simeq \left(\frac{\Delta\nu}{\Delta\nu_\odot}\right)^{12/5}\left(\frac{\nu_{\rm max}}{\nu_{\rm max,\odot}}\right)^{-14/5}\left(\frac{L}{\mathrm{L}_\odot}\right)^{3/10}. \quad (18)$$

To utilize these equations the effective temperatures and bolometric corrections for the stars are needed and for this we employed the calibration by Casagrande & VandenBerg (2014). We used V magnitudes from Milliman et al. (2014) except for two stars that were not in that catalogue and therefore obtained from Hole et al. (2009) (see caption of Table A3). Combining these with K_s magnitudes from the 2MASS catalogue (Cutri et al. 2003b) we calculated the $V-K_s$ colour-index and adopted a *nominal* reddening value of $E(B-V) = 0.15$ to get bolometric corrections and intrinsic colours using codes and tables from Casagrande & VandenBerg (2014). The reddening choice was made such that the $T_{\rm eff}$ obtained from the $V-K_s$ colour for the star KIC 5024327 is in exact agreement with a preliminary measurement from high resolution spectroscopy employing the asteroseismic $\log(g)$ value, 4790 K, (Slumstrup et al., in prep.) yielding also [Fe/H] $= +0.02 \pm 0.10$ which we adopted in the colour-temperature transformations. The reddening value so obtained is identical to that derived by (Bragaglia et al. 2001).

The procedure was done iteratively, making use of $\log(g)$ from the asteroseismic scaling relations as input for the transformations. We tested whether employing the differential reddening map of Platais et al. (2013) would improve our results, but found that this did not decrease the scatter in our measured masses and distance moduli, suggesting that the precision of the map is not high enough to improve relative $T_{\rm eff}$ estimates for the stars in our sample and we therefore neglected potential differential reddening effects. We note that our later assumption that all the stars should have the same *apparent* distance modulus is also better this way, since any real differences in the apparent distance modulus caused by differential interstellar absorption effects will be compensated by a slightly offset effective temperature due to differential interstellar reddening.

These choices result in our temperature scale which is on average 34 K hotter than the photometric scale of Lee-Brown et al. (2015) based on $B-V$ from several sources and 15 K hotter than the IRFM scale of Casagrande et al. (2014), in both cases with an RMS scatter of 35 K. Interestingly, if we adopt the $b-y$ colours from Casagrande et al. (2014) along with the calibration of Ramírez & Meléndez (2005) and their $E(b-y) = 0.74{\cdot}E(B-V)$ we obtain a temperature scale which is instead hotter than ours by 48 K with an RMS scatter of 50 K, partly due to the lower reddening value adopted by Casagrande et al. (2014) compared to us. The star KIC 5112491 is 33 K cooler on our scale than obtained by Bragaglia et al. (2001) using high-resolution spectroscopy (star 333) in a study that found a $\log(g)$ value only 0.06 dex higher than our asteroseismic measurement. KIC 5113061 is 34 K cooler on our scale compared to Thygesen et al. (2012) who used an asteroseismic $\log(g)$ value almost identical to ours to derive [Fe/H] $= +0.01$, very close to our adopted value mentioned above. Our $T_{\rm eff}$ scale is on average 55 K hotter than the one from spectroscopic measurements by APOKASC (Pinsonneault et al. 2014) for a subsample of the stars, with an RMS scatter of 62 K, when adopting their corrected ASPCAP temperatures. Their uncorrected ASCPCAP temperatures are on average 85 K cooler than ours.

Based on the very good agreement of our $T_{\rm eff}$ values with the other studies using various methods and calibrations we adopt an uncertainty of 50 K. While it is impossible to prove that this is true in an absolute sense, our later analysis certainly suggests that the estimate is conservative in a relative sense, since otherwise the scatter would be much larger in Fig. 11.

8.1 The distance modulus

For comparison purposes, the distance modulus to NGC 6819 and the mass of the RGB stars of the cluster can be measured from detached eclipsing binaries as it was done by Jeffries et al. (2013) and Sandquist et al. (2013). These distance measurements were redone by Brogaard et al. (2015) using the bolometric corrections from Casagrande & VandenBerg (2014) which we also employed for the giant stars in the present study. Brewer et al. (2016) added measurements of a third eclipsing cluster member and improved the analysis of the other two. The effective temperatures of the eclipsing components, which is currently determined from photometry, is the main uncertainty on the distance. Therefore, in order to put their distance modulus on the same scale as ours, we reestimated the effective temperature of the binary component WOCS 23009A using the same reddening and colour-temperature relations as for the giants. Since eclipse photometry does not exist for K_s the binary component colours could only be estimated for this one system where the secondary is so faint that the colours of the combined system is effectively the same as those of the primary component. We used the average result from $B-V$, $V-I$, and $V-K_s$ and obtained $(m-M)_V = 12.42 \pm 0.07$ where the uncertainty is taken from the range of results from each individual colour.

Fig. 9 shows the classical measures of apparent distance modulus, $(m-M)_V = 12.42 \pm 0.07$, and RGB mass (Brogaard et al. 2015; Sandquist et al. 2013), $M_{\rm RGB} = 1.55 \pm 0.06\,\mathrm{M}_\odot$ at the V-magnitude level of the RC and their 1-σ uncertainties (solid and dashed lines) along with the asteroseismic measurements of the individual giant stars, calculated using the scaling relations (Eq. 14 and Eq. 15). The

distance modulus of each giant is calculated using Eq. (10) in Torres (2010) with bolometric corrections from Casagrande & VandenBerg (2014).

Alternatively, we used also the surface-brightness-to-angular-diameter calibration of Di Benedetto (2005) to calculate the apparent distance modulus. This calibration is for $(V-K)$ to which we transformed our colours from $(V-K_s)$ using Carpenter (2001). This allows an interesting comparison, since the effective temperature only appears indirectly, and as a square-root term in the Di Benedetto (2005) calibration, whereas is goes as the fourth power in the luminosity term using Torres (2010). The latter approach gave distance moduli consistently lower by 0.06 mag compared to the former for most of the giants while a completely self-consistent value of $(m-M)_V = 12.47$ for the eclipsing component WOCS 23009A when comparing results from the two methods using $(V-K_s)$ (which is the reasonable thing to do, since systematic errors in colour should then affect each calibration similarly). At this level it is very difficult to identify the cause of discrepancy, since decreasing the giant effective temperatures by just 30 K in the former or increasing $E(B-V)$ by only 0.015 in the latter method would bring the distance moduli into exact agreement. Any small systematic error in either method or calibration of the photometry could contribute to the cause.

Most of the measurements in Fig. 9 are located along a tilted line because because the structure of the asteroseismic scaling relations is such that a measurement error that results in an overestimate of mass also results in an overestimate of radius and through that an overestimate of distance modulus. Stars are excluded from the calculation of mean values, if they have inferred distances deviating by more than 0.2 mag from the ensemble mean (e.g. KIC 5112786, see Fig. 9), are binaries, are not cluster members, or represent cluster stars that went through non-standard evolution (Corsaro et al. 2012; Brogaard et al. 2012, 2015). We discuss these stars in detail in §9.

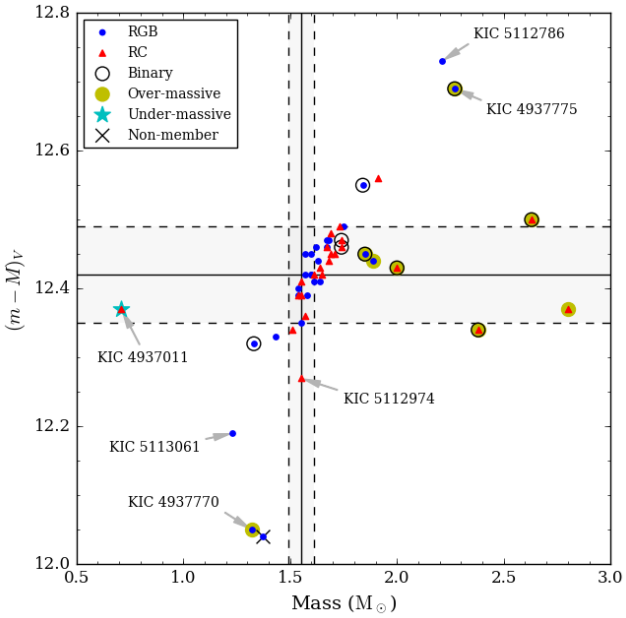

Figure 9. Distance modulus and mass for the cluster stars. In this plot a global correction of 2.54% was applied to $\Delta\nu$. Shaded regions denote the 1-σ intervals on the distance modulus and cluster mass (see text for details).

8.2 Corrections to $\Delta\nu$

Miglio et al. (2012) found that the asteroseismic scaling relation of $\Delta\nu$ to mean density is different for helium-burning RC stars compared to RGB stars due to a significantly different structure. Corrections to $\Delta\nu$ as a function of $T_{\rm eff}$ for RGB stars were suggested from model calculations by White et al. (2011). Miglio et al. (2013) extended such calculations all the way to the RC phase. In Fig. 9, an empirical positive correction of 2.54% was applied to $\Delta\nu$ of all the RGB stars. With this proposed correction to $\Delta\nu$ the mean distance moduli are identical for the groups of RGB and RC stars, respectively. Without the correction, the mean distance modulus to the RGB stars is larger by $\Delta DM = 0.11 \pm 0.02$ mag compared to that of the RC stars, which is very unlikely to be true since the two groups of stars belong to the same cluster. With the applied correction the mean distance modulus and mean mass of RGB stars is then also in satisfactory agreement with the measurements from the binary stars at the turn-off and main-sequence as seen in Fig. 9. The relative correction between RGB and RC stars is in excellent agreement with predictions in Miglio et al. (2013). However, those model predictions suggested that about half of the correction should be to RC stars in the negative direction. Our updated theoretically based corrections shown in Fig. 10b are different in that respect, being in very good agreement with the empirically derived result, also in an absolute sense. We therefore describe those corrections in some detail here while referring the reader to Rodrigues et al. (in preparation) for a full description.

To quantify how well the average large separation of radial modes adheres to the scaling with stellar mean density ($\rho/\rho_\odot \simeq (\Delta\nu/\Delta\nu_\odot)^2$), we calculated individual radial-mode frequencies for a set of stellar models ($M = 0.75$, 1.60, 2.50 $M_\odot$ and [Fe/H] = 0), using MESA (Paxton et al. 2013), from the zero-age main sequence to the first thermal pulse (see Bossini et al. (2015) and Rodrigues et al. (in preparation) for an exhaustive description of the models). Observational measurements of the average $\Delta\nu$ are limited by the number of frequencies identified around $\nu_{\rm max}$ and their uncertainties. Therefore, we must define a model-predicted $\langle\Delta\nu\rangle$ which is closest to how $\langle\Delta\nu\rangle$ is estimated from the data. Thanks to the measured individual radial-mode frequencies (see §5), we were able to construct the average $\Delta\nu$ from the models in a way that is consistent with that derived from the data. We defined $\langle\Delta\nu\rangle$ applying a linear fit as a function of n with weights defined as Gaussian function centred on $\nu_{\rm max}$ and of FWHM $= 0.66\,\nu_{\rm max}^{0.88}$ (Mosser et al. 2012a). We checked that this definition of $\langle\Delta\nu\rangle$ is within 1-σ of $\Delta\nu_{\rm fit}$.

Alternative definitions of $\langle\Delta\nu\rangle$ can be obtained by taking a weighted average of $\Delta\nu(\nu)$ itself. This however may lead to significant offsets (especially at low $\nu_{\rm max}$) depending on the reference frequency chosen to apply the weights to. We find the smallest offset if one associates to $\Delta\nu(\nu) = \nu_{n+1} - \nu_n$ the midpoint frequency between the ν_n and ν_{n+1}. This explains the difference at low $\nu_{\rm max}$ with the corrections

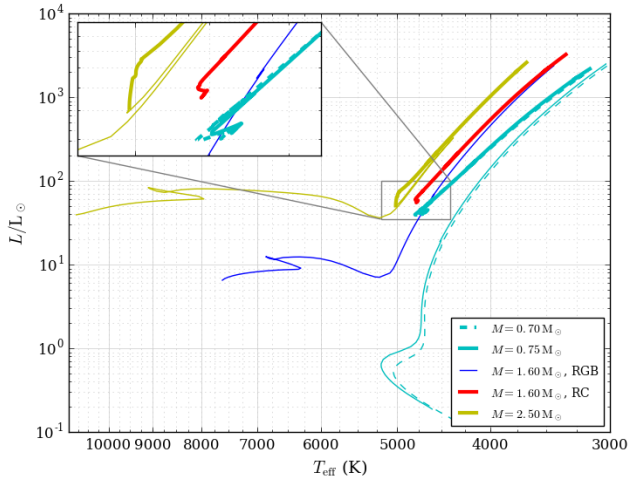

(a)

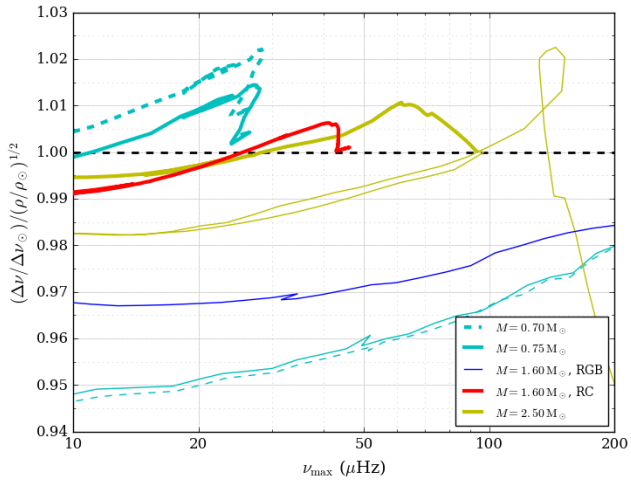

(b)

Figure 10. Stellar model evolutionary tracks for varying mass and [Fe/H] = 0. (a): Hertzsprung-Russell diagram. The insert shows the location of the RC. (b): Deviations from density-scaling for stellar models of selected masses.

presented in Miglio et al. (2013), where ν_n was chosen as at the reference frequency.

As is well known current models suffer from an inaccurate description of near-surface layers leading to a mismatch between theoretically predicted and observed oscillation frequencies. These so-called surface effects have a sizeable impact also on the large frequency separation, and on its average value. When utilising model-predicted $\Delta\nu$ it is therefore important to correct for such effects. As usually done, a first attempt at correcting is to use the Sun as a reference, hence by normalising the $\Delta\nu$ of a solar-calibrated model with the observed one. We have calibrated a solar model using the same input physics used in the tracks presented in Fig. 10a (see Rodrigues et al. in preparation for more details). By comparing the large frequency separation of our calibrated solar model and that from observed solar oscillation frequencies (Broomhall et al. 2014) we find that the predicted average ($\Delta\nu_{\rm mod} = 136.1\,\mu$Hz) is a 0.8% larger than the observed one ($\Delta\nu_{\rm obs} = 134.9\,\mu$Hz). We have therefore normalised the model predicted $\langle\Delta\nu\rangle$ to that of the calibrated solar model, leading to a model-suggested correction to $\Delta\nu$ as shown in Fig. 10b for stars positioned in the Hertzsprung-Russell diagram according to Fig. 10a.

In Fig. 11 we compare these theoretical corrections to empirical ones calculated from our measurements by assuming the distance modulus to be $(m - M)_V = 12.42$ and on a star-by-star basis adjusting $\Delta\nu$ until mass eqns. (16) and (17) (and therefore all four mass equations) yield the same mass. As seen, there is a general very good agreement between the theoretical and empirical correction with a scatter caused by errors in the measurements of $\Delta\nu$, $\nu_{\rm max}$, and $T_{\rm eff}$. The agreement strongly supports the theoretical corrections to $\Delta\nu$. This also suggests that no correction is needed for the other global parameter $\nu_{\rm max}$ (at least not at this metallicity). The fact that we are able, for the first time, to observationally confirm that the size of the $\Delta\nu$ correction changes with evolution up the RGB also shows that there is no significant evolutionary state dependent correction to $\nu_{\rm max}$ on the RGB. The agreement on the $\Delta\nu$ correction for both the RGB and RC phases also confirms that $\nu_{\rm max}$ should remain uncorrected, also for the RC phase of evolution.

By comparing the measured position relative to the theoretical prediction in Fig. 11, one can determine whether the star is on the RGB, in the RC, or an even later stage in evolution. This has important implications for the future exploitaion of asteroseismology of giant stars, since all that is needed is the global asteroseismic parameters $\Delta\nu$ and $\nu_{\rm max}$ and a distance measurement. With the latter expected from Gaia (Perryman et al. 2001) in the near future, this opens up the possibility to know the evolutionary state of stars without measuring the more difficult and observationally demanding gravity mode period spacing (Bedding et al. 2011), and thus it can be done for many more stars with less effort. This is also potentially very important for upcoming missions like TESS (Ricker et al. 2014), where individual frequencies can not be obtained for large fractions of the observed stars due to the limited time-coverage. Only one of the regular stars in NGC 6819 would be clearly misclassfied according to Fig. 11 (the RC star which falls on the RGB relation just below 50 μHz) while a few would be uncertain due to measurement errors. However, the identification becomes easier for stars of lower mass, since the $\Delta\nu$ correction varies more at lower masses. This allows a very clear classification as a RC star for an undermassive cluster member KIC 4937011, marked with a cyan star in Fig. 11 and described in detail in §9.1. We emphasize the potential of discriminating between the RGB, RC and AGB phases using only the asteroseismic parameters $\Delta\nu$ and $\nu_{\rm max}$ for any star with a known distance once future investigations verify that we can trust the correction to $\Delta\nu$ and that no correction to $\nu_{\rm max}$ is needed for all masses and metallicities that we are probing. Alternatively, for stars with a known distance where we can determine the evolutionary state independently, we can exploit the fact that we know the $\Delta\nu$ correction to obtain $T_{\rm eff}$ without the use of colours or spectra.

8.3 Mass loss

The mean masses of the RGB stars and RC stars in NGC 6819 were found to be $1.61 \pm 0.02\,M_\odot$ and $1.64 \pm$

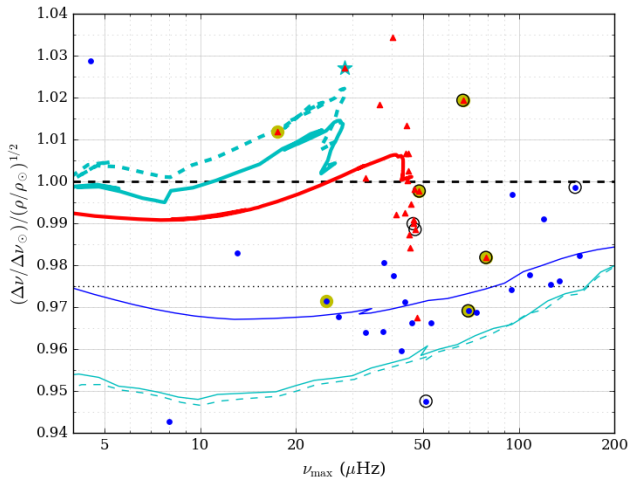

Figure 11. Comparison between theoretical and empirical corrections to scaling relations.

$0.02\,M_\odot$, respectively, independent of whether empirical or theoretical corrections to $\Delta\nu$ were used. A systematic uncertainty of at least the same level could be present, since changing $E(B-V)$ in our procedure by 0.01 mag (corresponding to about 25 K) changes the mean masses by $0.01\,M_\odot$. While such systematic uncertainties on e.g. effective temperatures add to the uncertainties of the absolute masses, the difference $\Delta M = -0.03 \pm 0.01$ is almost insensitive to systematics. We note in particular that we obtain the exact same value for ΔM when calculated using either of the Eqns. (15)–(18), one of which does not include $\Delta\nu$ and therefore independent of potential uncertainties in the correction of this parameter. This confirms the result of Miglio et al. (2012) of $\Delta M = -0.03 \pm 0.06$ between RGB and RC, but now with much higher confidence. A commonly used mass-loss law is that of Reimers (1975):

$$\frac{dM}{dt} = 4 \times 10^{-13} \eta_{\rm R} \frac{LR}{M}\,, \qquad (19)$$

where L, R, and M are the stellar luminosity, radius and mass in solar units, and $\eta_{\rm R}$ is a constant with units $M_\odot$ yr^{-1}. Isochrone comparisons to our measured ΔM like in Fig. 7 of Miglio et al. (2012) suggest $\eta_{\rm R}$ in the range 0 to 0.1 with a preference for 0. This is much lower than $\eta_{\rm R} = 1.4$ suggested by the calibration by Kudritzki & Reimers (1978) and also significantly lower than the value of $\eta_{\rm R}$=0.4 often adopted for globular clusters (see e.g. Renzini & Fusi Pecci 1988).

Schröder & Cuntz (2005) derived a more physically motivated mass-loss formula:

$$\frac{dM}{dt} = \eta_{\rm SC} \frac{LR}{M} \left(\frac{T_{\rm eff}}{4000\,{\rm K}}\right)^{3.5} \left(1 + \frac{g_\odot}{4300 \times g_\star}\right), \qquad (20)$$

with L, R, and M defined as before, $T_{\rm eff}$ and $g_\star$ the effective temperature and surface gravity of the star and $g_\odot$ the surface gravity of the Sun. In this case, $\eta_{\rm SC} = 8 \times 10^{-14}$ $M_\odot$ yr^{-1}. This is in conflict with our measurement since, without a recalibration of the constant $\eta_{\rm SC}$ in their relation, it predicts about the same mass loss for NGC 6819 as Reimers with $\eta_{\rm R} = 0.4$. However, such a recalibration would cause the relation to be in conflict with more direct measurements of mass-loss rates which match well the relation with the current value of $\eta_{\rm SC}$ (Schröder & Cuntz 2007).

It is interesting to note that if the RGB mass-loss in NGC 6791 also remains at the same value as derived by Miglio et al. (2012) when rederived with higher precision through the same procedure as ours for NGC 6819, then results on the two clusters NGC 6791 and NGC 6819 together suggest a much stronger mass dependence for the RGB mass-loss than suggested by the current formulations.

The measured masses of both RGB and RC stars are matched extremely well by a PARSEC isochrone of solar metallicity, no RGB mass-loss and an age of 2.25 Gyr — an age also in close agreement with that derived from eclipsing binary stars by Brewer et al. (2016) and from the white dwarf cooling sequence by Bedin et al. (2015).

9 STARS THAT EXPERIENCED NON-STANDARD EVOLUTION

We attribute a membership classification to the stars based on the radial-velocity (RV) and proper-motion (PM) study by Milliman et al. (2014) combined with our asteroseismic distance and mass measurements. In Table A2 a full list of classifications of the analysed stars is given. With regards to the nomenclature on cluster membership we use the following extended convention: 'S' and 'B' respectively denotes single and binary stars, 'O' and 'U' denoting over- or under-massive and 'M' or 'N' denoting member or non-member of NGC 6819. As an example, 'BOM' would denote a binary over-massive star that is a cluster member.

9.1 KIC 4937011 – a Li-rich low mass red clump member

The star KIC 4937011 has a 90% proper-motion probability of being a cluster member according to Sanders (1972) and was classified as a radial-velocity cluster member by Hole et al. (2009). However, an asteroseismic analysis by Stello et al. (2011) classified the star as a non-member. Anthony-Twarog et al. (2013) found this star to be lithium-rich and argued that it could be a cluster member red giant below the RGB bump and that the asteroseismic mis-match found by Stello et al. (2011) might be due to the star being in a special evolutionary stage. Recently, Milliman et al. (2014) published an updated radial velocity membership study of NGC 6819 that also contains the proper-motion membership information from Platais et al. (2013). While in that study KIC 4937011 remains a radial velocity member, the proper motion membership is 0%, in great contrast to the result from Sanders (1972), causing additional confusion about the cluster membership. Carlberg et al. (2015) investigated KIC 4937011 in greater detail with their evidence pointing strongly towards cluster membership.

Our asteroseismic analysis revealed that KIC 4937011 is a RC star according to the mixed-mode period spacing (Bedding et al. 2011). However, in accordance with Carlberg et al. (2015) we found KIC 4937011 to have a low-mass of $0.71 \pm 0.08\,M_\odot$, much lower than the other RC stars in the cluster. Given a negative correction to $\Delta\nu$ of 1.5% relative to the other RC stars, as suggested by Fig. 10b and Miglio et al. (2013) for such low-mass RC stars, the star has

self-consistent mass estimates from the four different mass-equations above for a star located at the cluster distance (See cyan star in Fig. 9). While this does not prove that the star is a cluster member, it is strongly suggestive. The position of the star in the CMD of Fig. 3 is also consistent with that of a RC star with a much lower mass than the other RC stars in the cluster, which we have confirmed by comparing to ZAHB loci in Rosvick & VandenBerg (1998). Although not evident from the publication, we have checked that a RC star with a mass of $0.71 \pm 0.08\,M_\odot$ would be located very near but a bit fainter than the reddest point of the ZAHBs they presented (D. A. VandenBerg, private communication), in excellent agreement with the relative magnitude and colour between KIC 4937011 and the other RC stars, and the predicted relative positions in the HR diagram of Fig. 10a. Since the star also has both [Fe/H] and [α/Fe] very similar to the other cluster stars according to measurements from the APOGEE survey (Carlberg et al. 2015), it seems very likely that KIC 4937011 is a cluster member in the RC phase of evolution that for some reason experienced enhanced mass-loss. Since the star was found to be a lithium-rich giant by Anthony-Twarog et al. (2013), this might indicate that the lithium production is related to the high mass-loss, a clue that might help solve the general puzzle of lithium-rich giants, as discussed e.g. by Silva Aguirre et al. (2014). KIC 4937011 is to the best of our knowledge only the third lithium-rich giant to be examined by asteroseismology[1], and the second one to be confirmed as a RC star. The strong indication that this star experienced higher-than-average mass-loss was only possible because it can be compared to other cluster members and thus demonstrates the importance of star clusters as asteroseismic science labs. It also highlights the caution that needs to be taken when age-dating RC stars in the field with asteroseismology, since some of them might have experienced higher-than-average mass-loss.

As an alternative to a higher than average mass-loss for KIC 4937011, the star could be a normal field RC giant that just happens to be located within the cluster. A repeat measurement using new observations of the proper-motion would be useful to determine whether it also moves with the cluster. In any case, the likelihood of having a chance overlap of an extremely old (as implied by the mass if mass-loss was normal; The age from the SAGA Survey is 14.7 ± 2 Gyr neglecting mass-loss (Casagrande et al. 2014)) solar-metallicity giant and a solar-metallicity cluster of much younger age seems very small.

9.2 Cluster members with above average mass

As seen in Fig. 9 there are a number of stars located at the cluster distance but with a higher mass than most of the stars. One cannot just dismiss these as non-members since, in addition to being at the cluster distance, they are also found to also be both PM and RV members in the study by Milliman et al. (2014), many of them as long period SB1 binary members suggesting a mass-transfer origin for the higher mass.

[1] The other two being KIC 9821622 (Jofré et al. 2015) and KIC 5000307 (Silva Aguirre et al. 2014).

We find a total of 6 overmassive giant members in our sample of 51 cluster members. While this is not a complete sample it strongly indicates that more than 10% of the giants in NGC 6819 are overmassive compared to the ensemble. We note that there are even more suspected overmassive candidates in the so-called superstamps observed in the central cluster region by *Kepler* but not yet exploited for this purpose. Our interpretation of these over-massive giants is that they underwent non-standard evolution through mass-transfer in a blue-straggler phase. This prevents estimates of age from their masses. Whether or not a similar number of over-massive giants is to be expected for field stars depends on whether binary fractions are significantly different in the field compared to open clusters and whether NGC 6819 can be considered a typical cluster in this respect. An additional complication is that most of the over-massive stars identified in NGC 6819 belong to very long period binary systems. Therefore it is not clear how the percentages will change for samples of stars where binarity can be ruled out. The potential appearance of a significant fraction of over-massive stars arising from non-standard evolution is certainly something that should be kept in mind when deriving asteroseismic ages for giant stars, especially when finding younger stars than expected. A good example of this is the 'Young α-rich stars' found by Chiappini et al. (2015) and Martig et al. (2015) which are now thought to be the result of mass-transfer rather than young age due to follow-up spectroscopy identifying many of them as long-period binaries (Yong et al. 2016; Jofre et al. 2016), exactly like the majority of the over-massive stars in our sample.

We discuss the individual over-massive giants below, referring to measured and derived values in tables A1–A3.

KIC 5024272

This star is a high probability PM and RV single member (Milliman et al. 2014) with an asteroseismic distance consistent with the cluster but a mass of about 2.8 $M_\odot$, much larger than the average RGB mass of 1.61 ± 0.02. This suggests that the giant formed from two stars that merged to form a massive single star. The single member status determined by (Milliman et al. 2014) is based on a total of 8 radial velocity measurements from two different telescopes, 4 epochs at each location covering well separated intervals of about 1000 days, and with about 5000 days between observations at the two telescopes. Still, due to measurement uncertainties and the unknown inclination of a potential binary orbit, a binary companion cannot be completely ruled out without further investigation. If a companion exists, it would have a mass below 0.4 $M_\odot$ (twice the turn-off mass minus the present mass of the overmassive star) if the system formed from a binary.

The CMD location about 1.5 mag brighter in V than the RC (brightest star in Fig. 3) is consistent with either the RGB or the AGB evolutionary phase. By making use of the four mass equations and relying on the predicted correction to $\Delta\nu$ for the RGB and AGB phase (Fig. 10b), respectively, for a star of this approximate mass we find a slight preference for the AGB phase, since that requires the smallest correction to reddening (and thus $T_{\rm eff}$) or $\nu_{\rm max}$ in order for all four mass equations to yield the same mass. If we assume that it is $T_{\rm eff}$ which needs a correction due to e.g. differen-

tial reddening or errors in the colour measurement then $T_{\rm eff}$ needs to be higher than our measurement by about 30 K for the AGB phase scenario and about 60 K higher for the RGB scenario. This suggests that if anything our $T_{\rm eff}$ is underestimated. This would also explain why Lee-Brown et al. (2015) who used a $T_{\rm eff}$ which is 145 K lower than our measurement obtained a low value of [Fe/H] $= -0.37$ since a higher $T_{\rm eff}$ would also result in a higher [Fe/H] more consistent with the average cluster metallicity.

KIC 5023953

This is another high probability PM and RV member, this time of SB1 type (Milliman et al. 2014). We classified this star as a RC star from the observed period spacing and its location in the RC in the CMD, which is also supported by the self-consistency of the mass from the four equations without applying a correction to $\Delta\nu$ (See Fig. 10b). It has very similar values of $\Delta\nu$ and ε_c compared to the other RC stars, but it has a higher mass, $M = 1.83 \pm 0.10\,{\rm M}_\odot$. This only agrees with expectations if the star is in a late core-helium-burning phase (see Fig. 4 in Stello et al. 2013).

KIC 5112880

Our analysis shows this to be an overmassive RGB star at cluster distance with a self-consistent asteroseismic mass of $M = 1.90 \pm 0.14\,{\rm M}_\odot$, in agreement with the single member status of Milliman et al. (2014).

KIC 5112361

This is an overmassive star at the cluster distance with $M = 1.85 \pm 0.06\,{\rm M}_\odot$ and a SB1 binary member according to (Milliman et al. 2014). The star is mentioned as outlier A in the $\Delta\nu - \Delta P$ diagram by Corsaro et al. (2012). However, our estimate of the observed period spacing is close to 60 seconds and thus we see no disagreement with either the theoretical or empirical prediction for the RGB phase (see Fig. 4 in Stello et al. 2013). The correction to $\Delta\nu$ (Fig. 10b) also supports the RGB phase, since assuming RC for the correction results in discrepant masses from the four equations and a too large distance modulus.

KIC 5024476

With a mass close to $M = 2.38\,{\rm M}_\odot$ this giant is overmassive and also an SB1 binary member (Milliman et al. 2014). It is mentioned as outlier D in the $\Delta\nu - \Delta P$ diagram by Corsaro et al. (2012). In general it is more difficult to use the $\Delta\nu - \Delta P$ diagram to distinguish between RGB and helium-burning phases for such high mass stars because the RGB phase of high mass stars also displays and increased period spacing (see Fig. 4 in Stello et al. 2013). However, in this case, the value found by Corsaro et al. (2012) is high enough that a core-helium burning secondary clump (2C) phase can be inferred when combined with the high mass. To support this further, we investigated the mass self-consistency using the theoretical correction to $\Delta\nu$ according to Fig. 10b assuming either an RGB or 2C scenario.

For both cases a correction to $T_{\rm eff}$ was also needed, +27 K for the secondary clump (2C) phase, +102 for RGB. The $T_{\rm eff}$ correction for the RGB case is at the 2σ level. Additionally, the resulting $T_{\rm eff}$ for the RGB scenario is almost 200 K hotter than the RGB evolutionary track for $M = 2.38\,{\rm M}_\odot$ at the measured luminosity, whereas for the 2C scenario the $T_{\rm eff}$ is only 28 K cooler than the model prediction from Fig. 10a. We take this as further confirmation that the star is in the 2C phase.

We derived the minimum mass of the secondary component from the semi-amplitude of the spectroscopic orbit from Milliman et al. (2014) and the asteroseismic mass of the giant component. If we assume that the system originates from two normal stars in the cluster then we can also estimate the maximum mass of the secondary component as the difference between the mass of the giant and two stars of the turn-off mass at about the time when the two stars started the mass transfer $(2 \times 1.61 - 2.38), {\rm M}_\odot = 0.84\,{\rm M}_\odot$. Since the minimum mass turns out to be as high as $0.6\,{\rm M}_\odot$ we have the absolute mass of the secondary component constrained to be 0.6–0.84 $\,{\rm M}_\odot$ consistent with the mass of a white dwarf in NGC 6819 according to Bedin et al. (2015).

The distance modulus for KIC 5024476 is different by 0.44 mag between the two distance measures we use, which could be indicating that magnitudes and/or colours are affected by a secondary component. However, a white dwarf, which seems the only likely secondary star due to the need of significant mass-transfer and the secondary mass derived, would either be too faint to affect colours or cause and overestimate of $T_{\rm eff}$ of the giant if the white dwarf is still in an early hot phase. Our above investigation required a hotter $T_{\rm eff}$, not lower. We therefore take the discrepant value of the distance modulus from the surface-brightness method as a further indication that the giant is in the 2C and that the surface-brightness-to-angular-diameter calibration does not hold for massive core-helium burning giants.

KIC 5024414

This star is mentioned as outlier C in the $\Delta\nu - \Delta P$ diagram by Corsaro et al. (2012). It is an SB1 binary member (Milliman et al. 2014) with a mass of roughly $2.6\,{\rm M}_\odot$. As mentioned above it can be difficult to use the $\Delta\nu - \Delta P$ diagram to distinguish between RGB and secondary clump phases, since for such high mass stars both phases can appear in overlapping regions of the diagram (see Fig. 4 in Stello et al. 2013). However, in this case the observed period spacing is high enough (about 170 s) to give strong preference to the 2C scenario for this mass. The value of ε_c also indicates that the star is in the core-helium burning phase.

The distance modulus for this star is different by 0.57 mag between the two distance measures we use, indicating that magnitudes and/or colours could be affected by a secondary component. B01 derived a spectroscopic $T_{\rm eff}$ of 4740 K which is much lower than our photometric value of 5049 K, which also suggests that colours are not directly related to $T_{\rm eff}$ for this star. On the other hand, our photometric $T_{\rm eff}$ is in good agreement with helium burning stars of similar metallicity and mass in NGC 6811 as derived by Molenda-Żakowicz et al. (2014). Also, the theoretical correction to $\Delta\nu$ requires in this case only relatively small negative corrections $T_{\rm eff}$ to reach mass self-consistency, -39 K for RGB, -67 K for 2C, with the resulting $T_{\rm eff}$ most consis-

tent with the model for the 2C scenario. The fact that the measured $T_{\rm eff}$ seems to be close to the true value allows us to interpret the discrepant distance modulus from the surface-brightness-to-angular-diameter method as being caused by the calibration being invalid for massive core-helium burning giants.

As for KIC 5024476 we can constrain the mass of the secondary binary component which in this case turns out to be in the range 0.47–0.72$M_\odot$, again consistent with a white dwarf.

9.3 Members and non-members

KIC 5024143

A single non-member according to Milliman et al. (2014), based on PRV= 93% and PM= 0%. Everything but but proper motion points to membership, so we re-classify to SM.

KIC 4937257

This is a giant with a mass of 1.08 $M_\odot$ in the RC evolutionary phase. According to [Fe/H] measurements (see Table A3) it has a metallicity close to solar. From the distance modulus and CMD position (at $V = 14.23, V - K_s = 3.02$ in Fig. 3) this star is a clear non-member, located behind the cluster. Instead, this star turns out to be very similar to RC stars of another open cluster, NGC 188. Meibom et al. (2009) measured the turn-off mass of NGC 188 from an eclipsing binary member to be very close to 1.1 $M_\odot$. The mass of the RC stars will be close to that of the turn-off mass, since the slightly higher mass of the RGB will almost compensated by the RGB mass-loss before reaching the RC as demonstrated for another old open cluster NGC 6791 by Brogaard et al. (2012). By comparing the $V - K_S$ colour of KIC 4937257 to that of KIC 4937011, the low-mass RC star and the colour of the other RC stars in NGC 6819, taking into account their relative masses, we estimated that $E(B-V)$ is higher for KIC 4937257 compared to the NGC 6819 by about 0.006 magnitude. Applying this to our $T_{\rm eff}$ derivation, we obtained $T_{\rm eff} = 4600$ K which is also the preliminary spectroscopic temperature obtained for a RC star in NGC 188 (Slumstrup et al., in prep.). Employing the CMD of NGC 188 produced by Stetson, McClure & VandenBerg (2004) we estimate the V magnitude of the RC stars to be 12.4 mag. Adopting the apparent distance modulus from Meibom et al. (2009), $(V - M_V) = 11.24$ results in an absolute M_V magnitude of the RC stars of 1.16 mag. For comparison, M_V for KIC 4937257 is 1.07 mag, which is consistent when taking into account uncertainties in the photometries and distance moduli of the two clusters. Summarising all this, KIC 4937257 is a RC star located in the field behind NGC 6819 with mass, $T_{\rm eff}$, metallicity and absolute magnitude very similar to the RC stars of the old open cluster NGC 188. By extension, the age of KIC 4937257 should also be very close to that of NGC 188, 6.2 ± 0.2 Gyr (Meibom et al. 2009).

KIC 4937257 is an example of the rare case when proper motion, radial velocity and metallicity measurements all erroneously point to cluster membership.

KIC 5024043

A non-member according to Milliman et al. (2014), based on PRV= 94% and PM= 0%. Sanders (1972) has PM=65% which would cause doubts about membership without further information. However, the asteroseismic distance modulus is 0.4 mag lower than that of the cluster, the CMD position is in the cluster RC while the asteroseismic classification is RGB with a radius which is also lower than that of the RC cluster stars. The metallicity is also consistently lower than the cluster mean according to the three literature [Fe/H] measurements in Table A3. Based on this evidence we conclude that this is a foreground RGB star with a mass of $1.32 \pm 0.04\,M_\odot$.

KIC 5023889

The apparent distance modulus $(m - M)_V = 11.24$ for this RGB star is much shorter than the cluster distance $(m - M)_V = 12.42$ and it is also a single non-member according to (Milliman et al. 2014) based on based on PRV= 93% and PM= 0%. Shifting the CMD postion of the star in Fig. 3 with the relative distance moduli puts it right on the RGB sequence where it would be expected to end up if it was a member since the metallicity is about the same as the cluster (Table A3). Therefore, there is no indication that the reddening is significantly lower than the cluster and the $T_{\rm eff}$ should thus be reliable for the mass estimate of $M = 1.40 \pm 0.05\,M_\odot$.

Uncertain cases

KIC 5112974

On the mass-distance plane in Fig. 9 this single member (Milliman et al. 2014) RC star seems slightly deviant compared to the other RC stars, displaying a mass of 1.55 $M_\odot$ and $(m - M)_V = 12.27$. However, taking into account that this is an evolved RC star with a $\Delta\nu$ value lower than the vast majority of RC stars suggests a theoretical $\Delta\nu$ correction that lessons the tension. Allowing additionally for the $T_{\rm eff}$ to be 61 K hotter than our measurement would result in complete agreement with the mean mass and distance for the RC stars. We thus attribute the slightly discrepant values for this star to measurement errors.

KIC 5113061 and KIC 5112786

These stars are on the mass-distance slope expected for members with rather large errors in Fig. 9. In the CMD they are located on the upper RGB sequence. Consequently, they present low values of $\Delta\nu$ and $\nu_{\rm max}$, and thus relative uncertainties that are large enough that they are still consistent with cluster membership in agreement with their SM status according to Milliman et al. (2014).

KIC 4937770 and KIC 4937775

These stars are located bluer than the single member RGB and below the RC in the CMD. Thus, if they are members, they are expected to be overmassive RGB stars. A higher than average RGB mass would also explain the outlier status

of KIC 4937770 in Corsaro et al. (2012) (Outlier B) based on the $\Delta\nu - \Delta P$ diagram. While not considered by Corsaro et al., a higher mass can explain the ΔP value due to the fact that RGB stars with masses above about $2\,M_\odot$ do show a gravity mode period spacings higher than that of RGB stars of lower mass (see Fig. 4 in Stello et al. 2013).

However, both stars appear to be significantly off the cluster distance in Fig. 9, which complicates their interpretation. Their $T_{\rm eff}$ from $b-y$ is lower by $\sim$100 K compared to $V-K$ although the average difference for the ensemble is 50 K in the other direction, suggesting issues with the photometry. Furthermore, the uncertainties on the asteroseismic parameters are large and $\nu_{\rm max}$ is in the range where the specific choice of background fit can change the derived $\nu_{\rm max}$ by more than 1 sigma (see Fig. 2b; $\nu_{\rm max}$ range 80–110 μHz), which complicates the analysis further. The membership study by (Milliman et al. 2014) suggests membership for both, KIC 4937775 being a binary member and KIC 4937770 a single member, although with proper motion membership probability of only 16% for the latter.

10 SUMMARY, CONCLUSIONS AND OUTLOOK

Our extensive peakbagging effort on *Kepler* light curves of evolved red giant stars of the open cluster NGC 6819 allowed new insights into both the cluster and asteroseismology. The fundamental improvement obtained by measuring individual oscillation modes and constructing the global parameters from these, is that exactly the same can be done for stellar models. This means that we are actually comparing the same thing in the measurements and models – something that is not possible if only the global parameters are available (e.g. the power spectrum of the power spectrum). We would therefore argue that this method is much more *accurate*, even if the *precision* would be comparable.

We found a remarkable agreement between empirical and theoretical corrections to the asteroseismic scaling relations for the red giants in NGC 6819. To verify that this holds at other masses and metallicities high precision asteroseismic measurements of giant stars in more open clusters Brogaard et al. (2015) and/or giant stars in binary systems (e.g. Frandsen et al. 2013; Brogaard et al. 2016) should be explored.

In the cases of the studied 51 red giant stars, we find that there is an excellent agreement between $\Delta\nu_{\rm global}$, obtained by using the PSPS-method, and $\Delta\nu_{\rm fit}$, obtained from individual frequencies (see Fig. 5). This is of vital importance for the many stars where individual frequencies can not be obtained, as this means that $\Delta\nu_{\rm global}$ can be directly compared to the values from stellar models, be it with larger uncertainties than what can be obtained with individual frequencies. We do, however, find that a little care has to be taken with respect to $\nu_{\rm max}$ and its correlation with the treatment of the granulation noise background. Differences between $\nu_{\rm max}$ obtained from different choices of background models are small, but can introduce differences on the percent-level, which, in the era of precision asteroseismology, could introduce significant contributions to the errors on estimated masses of stars.

We confirmed what was previously shown for stellar models (e.g. Montalbán et al. 2010b,a, 2012), that the small frequency separation, $\delta\nu_{02}$, can be used to distinguish the stellar evolutionary state between RGB and RC stars. Furthermore, we identified a new potential way to also make this distinction based on the empirical correction to $\Delta\nu$ for stars with a known distance. Although more studies are needed to set the ranges of applicability, this opens promising opportunities for asteroseismology with the upcoming TESS and PLATO missions complemented by Gaia distances.

The mean masses of the RGB stars and RC stars in NGC 6819 are $1.61 \pm 0.02\,M_\odot$ and $1.64 \pm 0.02\,M_\odot$, respectively. While systematic uncertainties on e.g. effective temperatures add to these absolute masses, the difference $\Delta M = -0.03 \pm 0.01\,M_\odot$ is much better defined and almost insensitive to systematics. Assuming a Reimers mass-loss law, model comparisons suggest $\eta_{\rm R}$ in the range 0 to 0.1 with a strong preference for no mass-loss at all.

Some of the stars that are outliers relative to the ensemble are revealed to be overmassive members that likely evolved via mass-transfer in a blue straggler phase, and KIC 4937011 is identified as a low-mass Li-rich cluster member in the RC phase that experienced very high mass-loss during its evolution. Such over- and undermassive stars need to be considered when studying field giants, since the true age of such stars cannot be known and there is currently no way to distinguish them from normal stars. If NGC 6819 can be assumed representative of the general field star population then about 10% of all giant stars did not evolve a single stars.

Our finding of non-members among stars with high cluster membership probabilities from radial-velocity and proper motion information and four members among stars with proper motion membership of 0% remind us that these tools are statistical in nature and therefore not to be trusted blindly for individual stars. It seems that for the particular study by Milliman et al. (2014) especially a proper motion membership of 0% should be considered with caution.

The extracted asteroseismic parameters and individual frequencies for this unique sample of stars will be useful for additional future studies of asteroseismology and stellar evolution.

ACKNOWLEDGEMENTS

Funding for the Stellar Astrophysics Centre is provided by The Danish National Research Foundation (Grant DNRF106). The research was supported by the ASTERISK project (ASTERoseismic Investigations with SONG and Kepler) funded by the European Research Council (Grant agreement no.: 267864).

APPENDIX A: TABLES

Table A1. Extracted asteroseismic parameters.

KIC	WOCS[1]	$T_{\rm eff}$[2] (K)	Orders[3]	Background	$\langle\delta\nu_{02}\rangle$ (μHz)	$\langle\Gamma_{n0}\rangle$ (μHz)	$\nu_{\rm max}$ (μHz)	ε_c[4]	$\Delta\nu_c$[4] (μHz)	ε	$\Delta\nu$ (μHz)	$\Delta\nu_{\rm corr}$[5] (μHz)
4937011	7017	4669	0	(3)	—	—	28.34±0.44	—	—	—	4.08±0.10	3.98
4937056	2012	4788	0	(4)	—	—	47.28±0.62	—	—	—	4.76±0.12	4.82
4937257	9015	4601	5	(5)	0.57±0.01	0.24±0.01	34.54±0.24	1.02±0.16	4.10±0.10	0.87±0.04	4.18±0.02	—
4937576	5016	4542	7	(4)	0.46±0.01	0.10±0.01	32.94±0.26	0.97±0.03	3.54±0.02	1.06±0.06	3.51±0.03	3.64
4937770	9024	4930	0	(5)	—	—	87.19±1.29	—	—	—	7.96±0.19	—
4937775	9026	5060	0	(2)	—	—	91.82±0.75	—	—	—	7.30±0.18	—
5023732	5014	4588	6	(3)	0.41±0.01	0.10±0.02	27.20±0.26	0.88±0.14	3.12±0.06	1.00±0.08	3.08±0.03	3.19
5023845	8010	4845	6	(2)	1.09±0.02	0.11±0.01	108.47±0.57	1.22±0.06	8.91±0.05	1.26±0.04	8.87±0.04	9.08
5023889	4014	4698	7	(3)	0.70±0.01	0.13±0.01	54.40±0.27	1.12±0.02	5.34±0.01	1.08±0.04	5.37±0.02	—
5023931	7009	4718	8	(3)	0.64±0.02	0.19±0.02	51.14±0.62	1.01±0.06	4.91±0.04	1.18±0.06	4.83±0.03	5.10
5023953	3011	4802	5	(3)	0.70±0.02	0.11±0.02	48.69±0.32	0.87±0.00	4.79±0.00	1.06±0.10	4.71±0.05	4.72
5024043	8013	4796	5	(3)	0.74±0.01	0.10±0.01	56.24±0.24	1.09±0.00	5.60±0.00	1.05±0.05	5.62±0.03	—
5024143	7005	4836	5	(2)	1.22±0.04	0.15±0.02	119.76±1.13	1.21±0.05	9.65±0.05	1.22±0.03	9.64±0.03	9.73
5024240	8007	4950	4	(5)	1.44±0.03	0.15±0.02	150.29±2.19	1.26±0.06	11.97±0.06	1.26±0.03	11.97±0.03	11.99
5024272	3003	4664	4	(3)	0.29±0.04	0.08±0.02	17.49±0.29	0.66±0.20	2.01±0.05	0.75±0.13	1.99±0.03	1.96
5024297	8003	4673	5	(3)	0.58±0.01	0.08±0.01	46.29±0.22	1.02±0.06	4.58±0.03	1.03±0.04	4.57±0.02	4.73
5024312	13002	4816	6	(5)	0.98±0.02	0.13±0.02	94.80±0.63	1.21±0.07	8.06±0.05	1.29±0.04	8.01±0.03	8.23
5024327	11002	4790	6	(3)	0.71±0.02	0.18±0.02	45.02±0.36	0.92±0.07	4.75±0.04	0.97±0.05	4.73±0.03	4.70
5024404	3004	4707	5	(4)	0.67±0.03	0.19±0.04	47.00±0.30	1.02±0.24	4.77±0.14	1.00±0.08	4.78±0.04	4.79
5024405	4001	4775	5	(5)	1.03±0.02	0.19±0.03	95.36±0.89	1.17±0.05	8.26±0.04	1.18±0.02	8.25±0.01	8.28
5024414	6002	5049	6	(5)	0.73±0.03	0.24±0.03	78.82±0.40	0.88±0.13	6.56±0.08	1.13±0.08	6.43±0.05	6.55
5024476	1006	4945	0	(5)	—	—	66.80±0.54	—	—	—	5.78±0.14	5.67
5024512	3001	4826	7	(5)	0.82±0.01	0.09±0.01	73.56±0.39	1.09±0.06	6.69±0.04	1.14±0.06	6.65±0.04	6.87
5024582	9002	4859	0	(5)	—	—	46.60±0.35	—	—	—	4.74±0.12	4.79
5024583	7003	4627	6	(3)	0.52±0.01	0.08±0.01	37.59±0.21	0.97±0.10	3.89±0.05	0.97±0.04	3.89±0.02	4.04
5024601	4002	4716	7	(4)	0.55±0.02	0.13±0.02	33.12±0.43	0.85±0.02	3.71±0.01	0.93±0.06	3.68±0.03	3.67
5024750	1004	4468	0	(3)	—	—	13.10±0.30	—	—	—	1.78±0.05	1.81
5024851	2008	4087	0	(3)	—	—	4.18±0.06	—	—	—	—	0.75
5024967	6009	4754	6	(4)	0.68±0.04	0.15±0.02	45.66±0.45	0.86±0.03	4.77±0.02	1.14±0.08	4.63±0.05	4.71
5111718	8018	4932	6	(2)	1.29±0.02	0.23±0.03	134.26±0.62	1.27±0.09	10.52±0.09	1.30±0.03	10.50±0.03	10.75
5111940	5012	4741	7	(5)	0.66±0.01	0.12±0.01	53.12±0.33	1.04±0.05	5.18±0.03	1.14±0.06	5.14±0.03	5.32
5111949	4011	4811	7	(4)	0.69±0.03	0.16±0.02	46.81±0.29	0.83±0.13	4.89±0.07	1.05±0.07	4.78±0.04	4.83
5112072	9010	4929	5	(4)	1.25±0.02	0.13±0.02	125.51±0.54	1.22±0.04	10.04±0.03	1.25±0.03	10.02±0.03	10.27
5112288	2007	4793	7	(3)	0.66±0.02	0.14±0.02	47.85±0.36	0.88±0.18	4.82±0.10	1.14±0.07	4.70±0.04	4.86
5112361	4008	4898	6	(5)	0.78±0.02	0.14±0.02	69.34±0.32	1.08±0.08	6.18±0.04	1.14±0.04	6.15±0.02	6.34
5112373	5005	4779	4	(3)	0.65±0.03	0.10±0.02	44.14±0.32	0.87±0.20	4.67±0.12	0.87±0.08	4.66±0.05	4.63
5112387	3007	4778	6	(4)	0.63±0.02	0.16±0.03	44.91±0.28	0.93±0.06	4.72±0.03	0.95±0.04	4.71±0.02	4.70
5112401	3009	4732	0	(4)	—	—	36.45±0.33	—	—	—	4.04±0.11	3.97
5112467	6003	4778	0	(5)	—	—	45.96±0.27	—	—	—	4.70±0.12	4.72
5112481	1007	4126	0	(4)	—	—	5.59±0.08	—	—	—	—	0.92
5112491	10002	4802	5	(4)	0.72±0.02	0.13±0.02	44.58±0.29	0.92±0.19	4.71±0.09	0.99±0.04	4.68±0.02	4.62
5112730	4005	4760	6	(3)	0.66±0.02	0.14±0.02	43.85±0.35	0.88±0.18	4.60±0.10	1.09±0.08	4.51±0.05	4.54
5112734	12002	4607	6	(5)	0.53±0.01	0.14±0.02	40.49±0.24	1.02±0.11	4.13±0.06	1.00±0.05	4.14±0.03	4.23
5112744	5011	4634	5	(4)	0.56±0.01	0.11±0.02	43.90±0.27	0.98±0.02	4.43±0.01	1.04±0.06	4.41±0.03	4.54
5112786	5003	4245	3	(4)	0.18±0.01	0.12±0.01	8.01±0.10	0.01±0.19	1.10±0.04	0.01±0.19	1.10±0.04	1.22
5112880	2004	4545	4	(3)	0.34±0.02	0.16±0.03	24.84±0.18	0.81±0.06	2.83±0.02	1.06±0.12	2.75±0.05	2.84
5112938	2006	4773	6	(4)	0.69±0.03	0.12±0.02	44.84±0.29	1.06±0.21	4.69±0.12	1.13±0.07	4.66±0.04	4.66
5112948	5007	4642	6	(3)	0.56±0.01	0.09±0.01	42.75±0.29	0.99±0.05	4.30±0.02	1.10±0.04	4.25±0.02	4.43
5112950	3005	4714	5	(4)	0.62±0.02	0.11±0.02	41.18±0.34	0.88±0.19	4.38±0.09	1.08±0.08	4.30±0.04	4.33
5112974	4009	4698	6	(3)	0.66±0.02	0.14±0.02	40.26±0.32	0.95±0.14	4.32±0.09	0.97±0.07	4.32±0.04	4.17
5113041	4007	4607	6	(3)	0.52±0.01	0.11±0.02	37.82±0.26	1.02±0.01	3.97±0.00	0.97±0.07	3.99±0.03	4.07
5113061	1014	4156	0	(5)	—	—	4.54±0.19	—	—	—	0.83±0.02	0.80
5113441	12016	4884	5	(2)	1.41±0.02	0.14±0.02	155.35±0.91	1.31±0.00	11.68±0.00	1.28±0.02	11.70±0.02	11.91
5200152	3021	4876	8	(4)	0.70±0.02	0.14±0.01	45.33±0.32	0.93±0.33	4.76±0.19	1.11±0.05	4.68±0.03	4.74

[1] ID from Milliman et al. (2014).
[2] From $(V - K_S)$ using Casagrande & VandenBerg (2014) and a nominal reddening of $E(B - V) = 0.15$.
[3] Number of individual radial modes measured. If 0 only $\Delta\nu_{\rm global}$ was determined.
[4] Derived using only the three central radial modes. See Kallinger et al. (2012).
[5] Empirically derived on a star-by-star basis using the distance modulus derived from eclipsing binaries.

Table A2. Derived stellar properties.

KIC	WOCS	$T_{\rm eff}$ (K)	Radius[1] ($R_\odot$)	Mass[1] ($M_\odot$)	$(m-M)_V$[2] (1)	$(m-M)_V$[3] (2)	CLASS	PM[4] (%)	PRV[4] (%)	Mem[4] Lit.	Mem Our
4937011	7017	4669	9.27±0.50	0.71±0.08	12.37	12.31	RC	0	94	SN	SUM
4937056	2012	4788	11.16±0.60	1.74±0.20	12.47	12.41	RC	98	94	BM	BM
4937257	9015	4601	10.41±0.17	1.08±0.04	13.16	13.09	RC	81	84	SM	SN
4937576	5016	4542	13.28±0.26	1.67±0.08	12.47	12.40	RGB	97	90	SM	SM
4937770	9024	4930	7.09±0.35	1.31±0.14	12.04	11.98	RGB	5	93	SM	SOM
4937775	9026	5060	9.49±0.47	2.51±0.25	12.79	12.74	RGB	16	89	BM	BOM
5023732	5014	4588	14.29±0.35	1.60±0.09	12.45	12.39	RGB	99	93	SM	SM
5023845	8010	4845	7.07±0.09	1.61±0.05	12.41	12.35	RGB	99	94	SM	SM
5023889	4014	4698	9.39±0.12	1.40±0.05	11.20	11.14	RGB	0	93	SN	SN
5023931	7009	4718	11.09±0.22	1.84±0.09	12.55	12.49	RGB	99	58	BM	BM
5023953	3011	4802	11.28±0.27	1.83±0.10	12.33	12.27	RC	99	93	BM	BOM
5024043	8013	4796	8.93±0.12	1.32±0.04	12.01	11.95	RGB	0	94	SN	SN
5024143	7005	4836	6.60±0.09	1.55±0.06	12.35	12.29	RGB	0	93	SN	SM
5024240	8007	4950	5.44±0.09	1.33±0.07	12.32	12.26	RGB	94	88	BM	BM
5024272	3003	4664	23.46±0.92	2.80±0.25	12.37	12.31	RGB	99	94	SM	SOM
5024297	8003	4673	11.14±0.14	1.67±0.06	12.46	12.40	RGB	99	85	SM	SM
5024312	13002	4816	7.55±0.10	1.60±0.05	12.42	12.37	RGB	86	88	SM	SM
5024327	11002	4790	10.80±0.17	1.55±0.06	12.39	12.33	RC	99	93	SM	SM
5024404	3004	4707	10.93±0.23	1.64±0.08	12.43	12.37	RC	99	90	SM	SM
5024405	4001	4775	7.13±0.09	1.43±0.05	12.33	12.27	RGB	98	91	SM	SM
5024414	6002	5049	10.49±0.18	2.63±0.11	12.50	11.93	RC	99	94	BM	BOM
5024476	1006	4945	10.91±0.54	2.38±0.24	12.34	11.90	RC	99	94	BM	BOM
5024512	3001	4826	8.51±0.13	1.57±0.06	12.45	12.39	RGB	99	90	SM	SM
5024582	9002	4859	11.21±0.56	1.74±0.18	12.46	12.41	RC	99	93	BM	BM
5024583	7003	4627	12.43±0.16	1.68±0.06	12.47	12.41	RGB	95	93	SM	SM
5024601	4002	4716	13.04±0.29	1.65±0.09	12.42	12.36	RC	76	91	SM	SM
5024750	1004	4468	20.30±1.15	1.54±0.19	12.39	12.32	RGB	99	91	SM	SM
5024851	2008	4087	36.87±0.64	1.55±0.14	12.42	12.34	RGB	99	93	BM	BM
5024967	6009	4754	11.36±0.26	1.73±0.09	12.49	12.43	RC	98	89	SM	SM
5111718	8018	4932	6.31±0.07	1.60±0.05	12.42	12.36	RGB	99	93	SM	SM
5111940	5012	4741	10.21±0.16	1.62±0.06	12.46	12.40	RGB	98	94	SM	SM
5111949	4011	4811	11.00±0.21	1.67±0.07	12.46	12.40	RC	99	92	SM	SM
5112072	9010	4929	6.47±0.07	1.57±0.05	12.42	12.36	RGB	99	94	SM	SM
5112288	2007	4793	11.62±0.22	1.91±0.09	12.56	12.50	RC	99	92	SM	SM
5112361	4008	4898	9.47±0.11	1.85±0.06	12.45	12.39	RGB	98	88	BM	BOM
5112373	5005	4779	10.88±0.26	1.54±0.08	12.39	12.33	RC	98	93	SM	SM
5112387	3007	4778	10.83±0.14	1.55±0.05	12.41	12.35	RC	99	94	SM	SM
5112401	3009	4732	11.91±0.65	1.51±0.17	12.34	12.28	RC	99	94	SM	SM
5112467	6003	4778	11.16±0.58	1.68±0.18	12.44	12.39	RC	99	94	SM	SM
5112481	1007	4126	32.78±0.57	1.64±0.15	12.42	12.34	RGB	0	91	SN	SM
5112491	10002	4802	10.92±0.16	1.57±0.06	12.36	12.31	RC	97	94	SM	SM
5112730	4005	4760	11.54±0.27	1.71±0.09	12.45	12.39	RC	99	91	SM	SM
5112734	12002	4607	11.83±0.19	1.64±0.06	12.41	12.35	RGB	0	87	SN	SM
5112744	5011	4634	11.33±0.21	1.63±0.07	12.44	12.37	RGB	96	94	SM	SM
5112786	5003	4245	31.56±2.10	2.21±0.30	12.73	12.66	RGB	99	86	SM	SM
5112880	2004	4545	16.34±0.57	1.90±0.14	12.45	12.38	RGB	99	73	SM	SOM
5112938	2006	4773	11.06±0.22	1.61±0.07	12.42	12.36	RC	98	85	SM	SM
5112948	5007	4642	11.86±0.18	1.75±0.07	12.49	12.43	RGB	98	92	SM	SM
5112950	3005	4714	11.85±0.27	1.69±0.09	12.45	12.39	RC	99	94	SM	SM
5112974	4009	4698	11.48±0.27	1.55±0.08	12.27	12.21	RC	94	93	SM	SM
5113041	4007	4607	11.86±0.23	1.54±0.07	12.40	12.33	RGB	98	93	SM	SM
5113061	1014	4156	31.49±2.04	1.23±0.20	12.19	12.11	RGB	99	94	SM	SM
5113441	12016	4884	5.85±0.06	1.58±0.05	12.39	12.33	RGB	98	88	SM	SM
5200152	3021	4876	11.20±0.19	1.69±0.07	12.48	12.42	RC	21	92	SM	SM

[1] Derived using a correction to $\Delta\nu$ of 2.54% for RGB stars and no correction to RC stars. For over- and undermassive stars and non-members a correction based on Fig. 10 was employed.
[2] Using bolometric corrections from Casagrande & VandenBerg (2014).
[3] Using the calibration by Di Benedetto (2005).
[4] From Milliman et al. (2014).

Table A3. All $T_{\rm eff}$ are in units of K.

KIC	WOCS	V[1]	$(V-K_s)$	$(b-y)$[2]	$T_{\rm eff}$[3] $(V-K_s)$	$T_{\rm eff}$[4] $(b-y)$	SAGA[2] $T_{\rm eff}$	SAGA[2] [Fe/H]	Lee-Brown[5] $T_{\rm eff}$	Lee-Brown[5] [Fe/H]	APOGEE[6] $T_{\rm eff}$	APOGEE[6] [Fe/H]
4937011	7017	13.59	2.92	0.77	4669	4680	4730	−0.36	4636	−0.05	4620	−0.03
4937056	2012	13.12	2.79	0.72	4788	4823	4789	−0.26	4709	−0.13	4761	0.02
4937257	9015	14.23	3.02	0.79	4601	4637	4594	−0.32	4583	0.06	4650	0.05
4937576	5016	13.11	3.09	0.80	4542	4581	4545	−0.09	4569	−0.17	4573	0.05
4937770	9024	13.49	2.64	0.73	4930	4789	4925	−0.35	4952	−0.11	4877	−0.01
4937775	9026	13.45	2.51	0.68	5060	4961	5104	−0.88	5120	−0.18	—	—
5023732	5014	12.86	3.02	0.76	4588	4702	4565	0.40	4539	−0.05	4541	0.05
5023845	8010	13.98	2.73	0.69	4845	4936	4838	0.09	4779	−0.14	—	—
5023889	4014	12.36	2.89	0.74	4698	4773	4646	0.32	4604	−0.20	4568	0.15
5023931	7009	13.31	2.87	0.73	4718	4793	4707	−0.04	4646	−0.57	4648	0.06
5023953	3011	12.94	2.77	0.71	4802	4884	4772	0.12	—	—	4780	0.14
5024043	8013	13.13	2.78	0.70	4796	4891	4832	−0.29	4806	−0.28	4676	−0.19
5024143	7005	14.08	2.74	0.69	4836	4929	4876	−0.09	4839	−0.15	4818	0.06
5024240	8007	14.32	2.62	0.68	4950	4990	4943	−0.40	4950	−0.05	4864	−0.09
5024272	3003	11.58	2.93	0.78	4664	4633	4568	0.16	4519	−0.37	—	—
5024297	8003	13.28	2.92	0.75	4673	4753	4619	0.11	4623	−0.15	—	—
5024312	13002	13.89	2.76	0.70	4816	4919	4795	−0.02	4781	−0.08	—	—
5024327	11002	13.11	2.79	0.71	4790	4860	4849	0.05	4731	−0.19	—	—
5024404	3004	13.24	2.88	0.75	4707	4750	4684	−0.24	4692	−0.07	—	—
5024405	4001	13.97	2.81	0.73	4775	4819	4714	−0.13	4739	−0.08	—	—
5024414	6002	12.95	2.52	0.66	5049	5045	4996	0.01	4946	−0.09	—	—
5024476	1006	12.83	2.62	0.68	4945	4979	4950	−0.26	—	—	4880	0.11
5024512	3001	13.64	2.75	0.70	4826	4912	4740	−0.01	4790	−0.16	—	—
5024582	9002	13.01	2.71	0.69	4859	4929	4822	−0.12	—	—	—	—
5024583	7003	13.12	2.98	0.76	4627	4708	4609	0.13	4567	−0.06	—	—
5024601	4002	12.83	2.87	0.74	4716	4776	4678	0.02	4677	−0.09	—	—
5024750	1004	12.22	3.18	—	4468	—	—	—	4393	−0.20	—	—
5024851	2008	11.69	3.79	0.97	4087	4108	4063	0.64	—	—	4174	0.09
5024967	6009	13.15	2.83	0.72	4754	4823	4749	−0.15	4744	0.00	4705	0.07
5111718	8018	14.12	2.64	0.67	4932	4997	4914	0.03	4890	0.00	4860	0.14
5111940	5012	13.37	2.84	0.73	4741	4819	4718	0.11	4688	−0.09	4632	0.06
5111949	4011	13.11	2.76	0.72	4811	4850	4776	0.12	4731	−0.03	4670	0.10
5112072	9010	14.07	2.64	0.67	4929	5004	4901	0.03	4865	−0.20	4841	0.04
5112288	2007	13.12	2.78	0.74	4793	4770	4787	−0.14	4716	−0.07	—	—
5112361	4008	13.31	2.67	0.70	4898	4912	4869	−0.39	4900	−0.35	—	—
5112373	5005	13.11	2.80	0.73	4779	4813	4729	0.00	4681	−0.02	4664	0.06
5112387	3007	13.14	2.80	0.73	4778	4799	4746	−0.09	4709	−0.13	4684	0.05
5112401	3009	12.93	2.85	0.73	4732	4819	4720	0.01	4722	−0.13	—	—
5112467	6003	13.11	2.80	0.71	4778	4853	4785	0.05	4714	−0.11	—	—
5112481	1007	11.86	3.71	—	4126	—	—	—	4149	−0.21	4265	0.05
5112491	10002	13.04	2.77	0.71	4802	4857	4782	−0.17	4752	−0.06	4755	0.03
5112730	4005	13.07	2.82	0.75	4760	4753	4733	−0.24	4714	−0.14	4693	0.09
5112734	12002	13.20	3.00	0.75	4607	4727	4683	−0.01	4639	−0.15	4585	0.09
5112744	5011	13.28	2.97	0.76	4634	4692	4643	−0.11	4645	−0.22	4601	0.03
5112786	5003	12.01	3.51	0.89	4245	4315	4249	0.11	4233	−0.18	—	—
5112880	2004	12.63	3.08	0.79	4545	4605	4497	0.10	4500	−0.04	4568	0.05
5112938	2006	13.11	2.81	0.73	4773	4796	4756	−0.08	4724	−0.11	—	—
5112948	5007	13.22	2.96	0.76	4642	4715	4643	0.02	4646	−0.13	—	—
5112950	3005	13.08	2.87	0.75	4714	4750	4756	−0.01	4666	−0.16	4667	0.09
5112974	4009	12.99	2.89	0.74	4698	4773	4650	−0.24	4710	−0.07	4686	0.04
5113041	4007	13.18	3.00	0.75	4607	4724	4587	0.03	4618	−0.13	4598	0.01
5113061	1014	11.65	3.66	0.96	4156	4141	4161	0.16	4113	−0.28	—	—
5113441	12016	14.32	2.69	0.68	4884	4990	4837	0.20	4882	0.03	4842	0.13
5200152	3021	13.00	2.69	0.72	4876	4846	4849	−0.31	4845	0.00	4753	0.08

[1] From Milliman et al. (2014) except for KIC 5112481 and KIC 5113061 which are from Hole et al. (2009).
[2] Casagrande et al. (2014).
[3] From $(V-K_S)$ using Casagrande & VandenBerg (2014) and a nominal reddening of $E(B-V)=0.15$.
[4] Using $(b-y)$ from Casagrande et al. (2014), $E(B-V)=0.15$ and colour-$T_{\rm eff}$ calibration by Ramírez & Meléndez (2005).
[5] Lee-Brown et al. (2015).
[6] Pinsonneault et al. (2014).

References

Anthony-Twarog B. J., Deliyannis C. P., Rich E., Twarog B. A., 2013, The Astrophysical Journal Letters, 767, L19
Appourchaux T. et al., 2014, Astronomy & Astrophysics, 566, A20
Appourchaux T. et al., 2012a, Astron. Astrophys., 537, A134
Appourchaux T. et al., 2012b, Astron. Astrophys., 543, 83
Basu S. et al., 2011, Astrophys. J., 729, L10
Bedding T. R. et al., 2011, Nature, 471, 608
Bedin L. R., Salaris M., Anderson J., Cassisi S., Milone A. P., Piotto G., King I. R., Bergeron P., 2015, Monthly Notices of the Royal Astronomical Society, 448, 1779
Borucki W. J., 2016, Reports Prog. Phys., 79, 036901
Borucki W. J. et al., 2010, Science (80-.)., 327, 977
Bossini D. et al., 2015, Mon. Not. R. Astron. Soc., 453, 2291
Bragaglia A. et al., 2001, The Astronomical Journal, 121, 327
Bressan A., Marigo P., Girardi L., Salasnich B., Dal Cero C., Rubele S., Nanni A., 2012, Monthly Notices of the Royal Astronomical Society, 427, 127
Brewer L. N. et al., 2016, ArXiv e-prints
Brogaard K. et al., 2016, ArXiv e-prints
Brogaard K., Sandquist E., Jessen-Hansen J., Grundahl F., Frandsen S., 2015, Astrophysics and Space Science Proceedings, 39, 51
Brogaard K. et al., 2012, Astronomy & Astrophysics, 543, A106

Broomhall A.-M., Chaplin W. J., Elsworth Y., Fletcher S. T., New R., 2009, Astron. Astrophys., 503, 241
Broomhall a.-M. et al., 2014, Mon. Not. R. Astron. Soc., 440, 1828
Brown T. M., Gilliland R. L., Noyes R. W., Ramsey L. W., 1991, Astrophys. J., 368, 599
Carlberg J. K. et al., 2015, Astrophys. J., 802, 7
Carpenter J. M., 2001, The Astronomical Journal, 121, 2851
Casagrande L. et al., 2014, The Astrophysical Journal, 787, 110
Casagrande L., VandenBerg D. A., 2014, Monthly Notices of the Royal Astronomical Society, 444, 392
Chiappini C. et al., 2015, Astron. Astrophys., 576, L12
Corsaro E., De Ridder J., 2014, Astronomy & Astrophysics, 571, A71
Corsaro E., De Ridder J., García R. A., 2015, Astronomy & Astrophysics, 579, A83
Corsaro E. et al., 2012, Astrophys. J., 757, 190
Cutri R. M. et al., 2003a, 2MASS All Sky Catalog of point sources.
Cutri R. M. et al., 2003b, 2MASS All Sky Catalog of point sources.
Davies G. R. et al., 2016, Monthly Notices of the Royal Astronomical Society, 456, 2183
Davies G. R., Handberg R., Miglio A., Campante T. L., Chaplin W. J., Elsworth Y., 2014, Mon. Not. R. Astron. Soc. Lett., 445, L94
Di Benedetto G. P., 2005, Monthly Notices of the Royal Astronomical Society, 357, 174
Dupret M.-a. et al., 2009, Astron. Astrophys., 506, 57
Elsworth Y., Hekker S., Basu S., Davies G.-R., 2016, Submitted to MNRAS
Frandsen S. et al., 2013, Astronomy & Astrophysics, 556, A138
Gaulme P. et al., 2016, The Astrophysical Journal Letters, 833, L13
Goupil M. J., Mosser B., Marques J. P., Ouazzani R. M., Belkacem K., Lebreton Y., Samadi R., 2013, Astron. Astrophys., 549, A75
Handberg R., 2013, Phd. thesis, Aarhus University
Handberg R., Campante T. L., 2011, Astron. Astrophys., 527, A56
Handberg R., Lund M. N., 2014, Mon. Not. R. Astron. Soc., 445, 2698
Harvey J., 1985, in ESA Futur. Mission. Solar, Heliospheric Sp. Plasma Phys., Rolfe E., Battrick B., eds., pp. 199–208
Hole K. T., Geller A. M., Mathieu R. D., Platais I., Meibom S. r., Latham D. W., 2009, Astron. J., 138, 159
Huber D. et al., 2011, Astrophys. J., 743, 143
Huber D. et al., 2010, Astrophys. J., 723, 1607
Jeffries, Jr. M. W. et al., 2013, The Astronomical Journal, 146, 58
Jofré E., Petrucci R., García L., Gómez M., 2015, Astronomy & Astrophysics, 584, L3
Jofre P., Masseron T., Izzard R. G., Van Eck S., Hawkins K., Jorissen A., Gilmore G., Paladini C., 2016, ArXiv e-prints
Kallinger T. et al., 2014, Astronomy & Astrophysics, 570, A41
Kallinger T. et al., 2012, Astron. Astrophys., 541, A51
Karoff C., 2008, PhD thesis, Aarhus University
Karoff C. et al., 2013, The Astrophysical Journal, 767, 34
Kjeldsen H., Bedding T. R., 1995, Astron. Astrophys., 293, 87
Kudritzki R. P., Reimers D., 1978, Astronomy & Astrophysics, 70, 227
Lee-Brown D. B., Anthony-Twarog B. J., Deliyannis C. P., Rich E., Twarog B. A., 2015, The Astronomical Journal, 149, 121
Lund M. N. et al., 2017, The Astrophysical Journal, 835, 172
Martig M. et al., 2015, Monthly Notices of the Royal Astronomical Society, 451, 2230
Meibom S. et al., 2009, Astron. J., 137, 5086
Miglio a. et al., 2012, Mon. Not. R. Astron. Soc., 419, 2077
Miglio a. et al., 2013, EPJ Web Conf., 43, 03004
Milliman K. E., Mathieu R. D., Geller A. M., Gosnell N. M., Meibom S., Platais I., 2014, The Astronomical Journal, 148, 38
Molenda-Żakowicz J., Brogaard K., Niemczura E., Bergemann M., Frasca A., Arentoft T., Grundahl F., 2014, Monthly Notices of the Royal Astronomical Society, 445, 2446
Montalbán J., Miglio A., Noels A., Scuflaire R., Ventura P., 2010a, Astron. Nachrichten, 331, 1010
Montalbán J., Miglio A., Noels A., Scuflaire R., Ventura P., 2010b, Astrophys. J., 721, L182
Montalbán J., Miglio A., Noels A., Scuflaire R., Ventura P., D'Antona F., 2012, Astrophys. Sp. Sci. Proc., 26, 23
Mosser B. et al., 2011, Astron. Astrophys., 525, L9
Mosser B. et al., 2012a, Astron. Astrophys., 537, A30
Mosser B. et al., 2012b, Astron. Astrophys., 540, A143
Paxton B. et al., 2013, Astrophys. J. Suppl. Ser., 208, 4
Perryman M. A. C. et al., 2001, Astron. Astrophys., 369, 339
Pinsonneault M. H. et al., 2014, The Astrophysical Journal Supplement Series, 215, 19
Platais I., Gosnell N. M., Meibom S., Kozhurina-Platais V., Bellini A., Veillet C., Burkhead M. S., 2013, The Astronomical Journal, 146, 43
Ramírez I., Meléndez J., 2005, The Astrophysical Journal, 626, 465
Reimers D., 1975, Memoires of the Societe Royale des Sciences de Liege, 8, 369
Renzini A., Fusi Pecci F., 1988, Annual Rev. Astron. Astrophys, 26, 199

Ricker G. R. et al., 2014, J. Astron. Telesc. Instruments, Syst., 1, 014003
Rosvick J. M., VandenBerg D. A., 1998, Astron. J., 115, 1516
Sanders W. L., 1972, Astron. Astrophys., 19, 155
Sandquist E. L. et al., 2013, The Astrophysical Journal, 762, 58
Schröder K.-P., Cuntz M., 2005, The Astrophysical Journal Letters, 630, L73
Schröder K.-P., Cuntz M., 2007, Astronomy & Astrophysics, 465, 593
Schwarz G., 1978, The Annals of Statistics, 6, 461
Silva Aguirre V. et al., 2014, The Astrophysical Journal Letters, 784, L16
Stello D., Chaplin W. J., Basu S., Elsworth Y., Bedding T. R., 2009, Mon. Not. R. Astron. Soc. Lett., 400, L80
Stello D. et al., 2013, The Astrophysical Journal Letters, 765, L41
Stello D. et al., 2011, Astrophys. J., 739, 13
Stetson P. B., McClure R. D., VandenBerg D. A., 2004, Publ. Astron. Soc. Pacific, 116, 1012
Tassoul M., 1980, The Astrophysical Journal Supplement Series, 43, 469
Thygesen A. O. et al., 2012, Astronomy & Astrophysics, 543, A160
Torres G., 2010, The Astronomical Journal, 140, 1158
Trampedach R., Asplund M., Collet R., Nordlund Å., Stein R. F., 2013, The Astrophysical Journal, 769, 18
Trampedach R., Stein R. F., Christensen-Dalsgaard J., Nordlund Å., Asplund M., 2014, Monthly Notices of the Royal Astronomical Society, 442, 805
Vrard M., Mosser B., Samadi R., 2016, Astronomy & Astrophysics, 588, A87
White T. R., Bedding T. R., Stello D., Christensen-Dalsgaard J. r., Huber D., Kjeldsen H., 2011, Astrophys. J., 743, 161
Yong D. et al., 2016, ArXiv e-prints